



**HAL**  
open science

## Land-use changes in Amazon and Atlantic rainforests modify organic matter and black carbon compositions transported from land to the coastal ocean

Tassiana Soares Gonçalves Serafim, Marcelo Gomes de Almeida, Gérard Thouzeau, Emma Michaud, Jutta Niggemann, Thorsten Dittmar, Michael Seidel, Carlos Eduardo de Rezende

### ► To cite this version:

Tassiana Soares Gonçalves Serafim, Marcelo Gomes de Almeida, Gérard Thouzeau, Emma Michaud, Jutta Niggemann, et al.. Land-use changes in Amazon and Atlantic rainforests modify organic matter and black carbon compositions transported from land to the coastal ocean. *Science of the Total Environment*, 2023, 878 ((2023)), pp.162917. 10.1016/j.scitotenv.2023.162917. hal-04303490

**HAL Id: hal-04303490**

**<https://hal.univ-brest.fr/hal-04303490v1>**

Submitted on 27 Aug 2024

**HAL** is a multi-disciplinary open access archive for the deposit and dissemination of scientific research documents, whether they are published or not. The documents may come from teaching and research institutions in France or abroad, or from public or private research centers.

L'archive ouverte pluridisciplinaire **HAL**, est destinée au dépôt et à la diffusion de documents scientifiques de niveau recherche, publiés ou non, émanant des établissements d'enseignement et de recherche français ou étrangers, des laboratoires publics ou privés.

## **Land-use changes in Amazon and Atlantic Rainforests modify organic matter and black carbon compositions transported from land to the coastal ocean**

Tassiana S.G. Serafim<sup>a\*</sup>, Marcelo G. Almeida<sup>a</sup>, Gérard Thouzeau<sup>b</sup>, Emma Michaud<sup>b</sup>, Jutta Niggemann<sup>c</sup>, Thorsten Dittmar<sup>c,d</sup>, Michael Seidel<sup>c</sup>, Carlos E. Rezende<sup>a</sup>

<sup>a</sup> Laboratório de Ciências Ambientais, Centro de Biociências e Biotecnologia, Universidade Estadual do Norte Fluminense Darcy Ribeiro, Campos dos Goytacazes RJ, CEP 28013-602, Brazil.

<sup>b</sup> Univ Brest, CNRS, IRD, Ifremer, UMR 6539 - LEMAR, F-29280 Plouzané, France.

<sup>c</sup> Research Group for Marine Geochemistry (ICBM-MPI Bridging Group), Institute for Chemistry and Biology of the Marine Environment, Carl von Ossietzky University Oldenburg, Germany.

<sup>d</sup> Helmholtz Institute for Functional Marine Biodiversity (HIFMB) at the University of Oldenburg, Germany

\* Corresponding author: Serafim, T.S.G., e-mail: [tassiana.sgs@gmail.com](mailto:tassiana.sgs@gmail.com)

1 **Abstract:** This study assessed black carbon (BC) dynamics, concentrations,  
2 and the organic matter (OM) isotopic carbon composition in northeastern South  
3 America drainage basin coastal sediments. Paraíba do Sul (PSR; Atlantic  
4 Rainforest, Brazil) coastal sediments displayed more  $^{13}\text{C}$ -enriched values ( $-22.6$   
5  $\pm 1.3$  ‰ [ $n = 13$ ]) than Amazon and Sinnamary (Amazon Rainforest in French  
6 Guiana and Brazil) sediments ( $-25.0 \pm 3.1$  ‰ [ $n = 14$ ] and  $-26.1 \pm 1.0$  ‰ [ $n = 6$ ],  
7 respectively), indicating that local land-use basin changes have altered the OM  
8 composition, *i.e.*, from natural  $\text{C}_3$  plant to  $\text{C}_4$  plants contributions. BC contents  
9 normalized to total organic carbon (TOC) content were  $0.32 \pm 0.24$  ( $n = 8$ ),  $0.73$   
10  $\pm 0.67$  ( $n = 6$ ), and  $0.95 \pm 0.74$  ( $n = 13$ )  $\text{mg g}^{-1}$  TOC for Amazon, Sinnamary and  
11 PSR samples, respectively, with BC sources appearing to differ according to  
12 different drainage basin vegetation covers. With increasing distance from the  
13 river mouths, BC contents exhibited different trends between the coastal zones,  
14 with values increasing for the PSR and decreasing values for the Amazon  
15 samples. BC distribution in Sinnamary coastal sediments did not display  
16 specific patterns. Regarding the Amazon coastal zone, BC contents decreased  
17 while the B6CA:B5CA ratios did not show a pattern, which could indicate that  
18 BC in the area originates from river transport (aged BC) and that the  
19 hydrophobic component of dissolved BC is removed. The BC content mostly  
20 increased in the PSR coastal zone, while the B6CA:B5CA ratios were not  
21 altered for the entire gradient, indicating the BC stability and possible  
22 atmospheric deposition of soot. Our findings indicate that different sources,  
23 transformation processes, and hydrological conditions affect BC contents within  
24 coastal zones. Continuous land cover changes in both the Amazon and Atlantic  
25 Rainforests may result in large-scale marine carbon cycling impacts.

26 Keywords: Black carbon; Amazon Rainforest; Atlantic Rainforest; Carbon  
27 isotopic composition; Coastal sediments; Organic matter.

## 28 1. INTRODUCTION

29 The conversions of primary forest areas to croplands and agricultural  
30 areas have devastated the Brazilian Atlantic Rainforest, destroying important  
31 biomes such as the world's largest forest, the Amazon Rainforest (Ferrante and  
32 Fearnside, 2019), modifying organic matter (OM) soil contents (Bernardes et al.,  
33 2004). Native forest vegetation conversion has altered the Atlantic Rainforest  
34 landscape, with about 28 % of the original vegetation cover now distributed only  
35 in fragments (Rezende et al., 2018; Solórzano et al., 2021). Such anthropogenic  
36 areas currently comprise approximately 15 % of the entire Amazon biome (Stahl  
37 et al., 2016), and are now on the rise due to the destruction of forest areas. One  
38 strategy applied to forest biomass removal and the management of  
39 anthropogenic regions consists in fire cleaning (Edwards, 1984). Fire is  
40 currently considered the primary Amazon Rainforest biomass removal vector,  
41 through forest fires caused by drought events (Aragão et al., 2018) or  
42 anthropogenic activities, such as cattle pasture expansion and management  
43 and agricultural activities. Wildfires and anthropogenic burning globally emit  
44 about 2.2 Pg of carbon per year in the form of greenhouse gases (Werf et al.,  
45 2017). Furthermore, fires also produce another carbon-enriched form displaying  
46 higher resistance to degradation than non-thermally-altered OM, named black  
47 carbon (BC) (Forbes et al., 2006; Bird and Ascough, 2012).

48 Black carbon is commonly described as the thermally altered and  
49 condensed aromatic OM fraction produced after incomplete combustion of plant  
50 biomasses or fossil fuels (Goldberg, 1985). Hedges et al. (2000) described the  
51 broad spectrum of BC compounds as a combustion continuum, later termed the  
52 degradation continuum (Bird et al., 2015), ranging from levoglucosan to highly

53 condensed aromatic compounds that may display environmental persistence  
54 (Wagner et al., 2021). The global production of BC derived from plant  
55 biomasses has been estimated as ranging between 50 and 300 Tg of BC per  
56 year (Forbes et al., 2006; Bird et al., 2015) and about 80 % of BC initially  
57 remains in BC production sites following combustion (Kuhlbusch and Crutzen,  
58 1995). According to Reisser et al. (2016), BC comprises about 14 % of overall  
59 soil OM, with an average residence time of 88 years. This residence time,  
60 however, can range from a few years to millennia, depending on the  
61 combination of physical, chemical, and microbial processes (Singh et al., 2012).  
62 Black carbon mobilization from soils and its entry into aquatic systems occurs  
63 mainly through the dissolved phase following solubilization of historical BC  
64 (Dittmar, 2008; Dittmar et al., 2012b) and lateral particle transport, mainly due to  
65 soil erosion (Major et al., 2010). In addition, BC inputs into aquatic systems can  
66 take place, to a smaller extent, via atmospheric transport, and its deposition can  
67 take place along the entire continent-ocean gradient (Jurado et al., 2008;  
68 Coppola et al., 2018).

69 Increased erosion due to land-use conversion increases particle  
70 transport into the aquatic system, resulting in the global accumulation of 75 Tg  
71 sediments per year, mainly in areas below 2000 m altitude (Wilkinson &  
72 McElroy, 2007). These eroded particles travel throughout the water column and  
73 eventually become deposited along the continent-ocean gradient, mainly in  
74 continental areas and transition zones, with only about 20 % of this suspended  
75 particulate matter (SPM) reaching their destination, the marine sediments (Bird  
76 et al., 2015; Coppola et al., 2018). The transport of SPM and associated OM  
77 along the continent gradient is influenced by river and drainage basin

78 characteristics (Burdige, 2007). Suspended particulate matter transport is faster  
79 in small rivers usually associated with mountains, narrow continental shelves, or  
80 active continental margins, resulting in relatively low OM remineralization rates  
81 along the continent-ocean gradient (Blair et al., 2003). In contrast, SPM is  
82 subject to deposition and resuspension cycles in large rivers, resulting in  
83 increased OM remineralization due to long residence times (Aller, 1998).  
84 Additionally, OM (and BC) transported alongside particles can be replaced  
85 downstream by OM produced at lower elevations (Aller et al., 1996; Burdige,  
86 2007).

87         By estimating BC contents associated with SPM and sediments of both  
88 large (e.g., the Amazon, Congo) and small (e.g., the Eel, Santa Clara, Danube)  
89 rivers, Coppola et al. (2018) reported that BC comprised about  $15.8 \pm 0.9$  % of  
90 total organic carbon (TOC) content, and the data did not indicate associations  
91 between BC contents and river size. Furthermore, BC export dynamics in the  
92 rivers were attributed to soil erosion, where BC generally undergoes constant  
93 pre-ageing despite environmental conditions and settings. However, SPM  
94 transport to the ocean is considerably reduced due to strong physicochemical  
95 gradients, favoring certain processes, such as flocculation, in estuarine zones  
96 (Eisma, 1986). Regnier et al. (2013) estimated that about 20 % of the TOC  
97 associated with SPM does not reach the open ocean, due to deposition along  
98 continent–coastal gradients. The global flux of particulate BC to the ocean  
99 ranges from 19 to 80 Tg per year (Bird et al., 2015), assuming that BC  
100 comprises between 5 and 15 % of the TOC content (Cole et al., 2007).  
101 Lohmann et al. (2009) reported that BC accounted for between 3 and 35 % of  
102 OC contents in deep-sea sediments from the South Atlantic Ocean. These

103 authors estimated the most recalcitrant form obtained by the degradation  
104 continuum model by isolating soot BC through the thermochemical oxidation  
105 technique and attributing its primary source as terrestrial by analyzing the  
106 isotopic organic carbon ( $\delta^{13}\text{C}$ ) composition. To evaluate environmental BC  
107 sources,  $\delta^{13}\text{C}$  values are often associated with BC content, as reported by Liu  
108 and Han (2021), who coupled BC content with  $\delta^{13}\text{C}$  results and reported that  
109 the main source of BC associated to SPM in the Xijiang River Basin, in  
110 Southeast China, is fossil fuel combustion, accounting for around 80 % of the  
111 total BC content.

112 In this context, BC spatial dynamics and concentrations were assessed  
113 in the coastal sediments of three northeastern South American drainage basins.  
114 The Sinnamary (French Guiana) and Amazon River (Brazil) basins are covered  
115 by primary forest vegetation (terrestrial  $\text{C}_3$  plants), whereas the Paraíba do Sul  
116 River (PSR; Brazil) basin is mainly covered with grasses (terrestrial  $\text{C}_4$  plants),  
117 due to land-use changes. We further evaluated if the transition from primary  
118 forests to pasture and cultivation areas has altered the sources and composition  
119 of the OM deposited in associated coastal sediments. Black carbon content was  
120 analyzed by the benzene-polycarboxylic acid (BPCA) method, and elemental  
121 and isotopic OM compositions of bulk total organic carbon (TOC and  $\delta^{13}\text{C}$ ), as  
122 well as nitrogen (N and  $\delta^{15}\text{N}$ ) were determined. Three hypotheses were tested:  
123 (1) the OM of the PSR is  $^{13}\text{C}$ -enriched compared to the Amazon River, due to  
124 vegetation basin cover alterations; (2) the BC content in the Amazon River  
125 coastal zone is lower compared to the other evaluated coastal sediments as a  
126 result of OM dilution and floodplain replacement; and (3) BC content is directly  
127 related to land use alterations in the PSR coastal zone and not to historical

128 Atlantic Rainforest burning, as suggested previously for dissolved BC (Dittmar  
129 et al., 2012; Marques et al. 2017).

## 130 **2. MATERIAL AND METHODS**

### 131 **2.1. Study areas**

#### 132 **2.1.1. The Amazon and French Guiana coastal zones**

133 The Amazon Rainforest extends over several countries, including Brazil  
134 and French Guiana. Its surface area represents about 45 % of the world's  
135 remaining tropical forests (Laurance et al., 2001), which comprises  
136 approximately 4 % of the Earth's surface (about 6,100,000 km<sup>2</sup>) (Malhi et al.,  
137 2008; Gallo and Vinzon, 2015). The Amazon Rainforest, besides playing an  
138 essential role in storing carbon in its biomass, is responsible for transporting  
139 terrestrial carbon to the Atlantic Ocean via the Amazon River (Cai et al., 1988;  
140 Malhi et al., 2006, 2008). The Amazon River exhibits a seasonal cycle with  
141 maximum discharge reaching an average of 209,000 m<sup>3</sup> s<sup>-1</sup> from May to July  
142 (Latrubesse, 2008). Material discharges to the coastal zone comprise  
143 approximately 20 % of the global input of terrestrial material to the ocean  
144 (Richey et al., 1986; Ward et al., 2015). Due to the basin's climate, strong  
145 erosion and rapid particle deposition processes can lead to rapid sedimentation  
146 rate changes in the Amazon River plume area (Kuehl et al., 1986). The plume  
147 moves in a northwestern direction, and it has been suggested that a large  
148 portion of the OM in the sedimentary compartment of the Brazilian shelf and  
149 adjacent northwestern areas originates from the Amazon basin (Wells and  
150 Coleman, 1981; Nittrouer et al., 1986). Approximately 20 % of the SPM  
151 reaching the coastal zone is carried towards French Guiana, due to interactions

152 between the Brazilian North Current, east trade winds, and semi-diurnal sea  
153 currents (Geyer et al., 1996; Aller et al., 2004).

154 French Guiana vegetation cover comprises 97 % of tropical forest  
155 (Chave et al., 2001), with extensive mangrove forests covering over 80 % of the  
156 coast (Fromard et al., 2004). The Sinnamary River is considered a small river,  
157 and its drainage basin extends over 6,565 km<sup>2</sup>, with seasonal river discharges  
158 (Richard et al., 2000; Ray et al., 2018). The minimum and maximum discharge  
159 averages range between 193 and 700 m<sup>3</sup> s<sup>-1</sup> in November (dry season) and  
160 June (wet season) 2015, respectively (Ray et al., 2018; source: DEAL  
161 GUYANE-EDF). According to Oliveira and Clavier (2000) and Merona (2005),  
162 water discharge variations in this area depends on the anthropogenic process  
163 of opening an upstream dam and the natural El Niño event. The Sinnamary  
164 River estuary undergoes a macro tidal regime, with a tidal range of ca. 3 m near  
165 the river mouth (Ray et al., 2018). The estuary's extensive mangrove forests are  
166 dominated by *Avicennia germinans* (Marchand et al., 2003, Marchand, 2017).

### 167 **2.1.2. The Paraíba do Sul coastal zone**

168 The Paraíba do Sul River (PSR) basin, comprising 57,000 km<sup>2</sup>, extends  
169 over the states of São Paulo, Rio de Janeiro, and Minas Gerais in southeastern  
170 Brazil (Ovalle et al., 2013). The PSR occupies an area previously entirely  
171 covered by Atlantic Rainforest, and about 74 % of its basin is currently covered  
172 by pasture and sugar-cane crop areas (Figueiredo et al., 2011; Marques et al.,  
173 2017). Due to these changes, the basin has suffered from intense erosion,  
174 leading to higher particle inputs to the local aquatic system. The PSR estuary  
175 and the second largest mangrove forest in the state of Rio de Janeiro are  
176 located in São João da Barra, in the Norte Fluminense region (Bernini and

177 Rezende, 2004). The PSR is a small- to a medium-sized river, whose  
178 discharges depend on the season. In the dry period, between June and  
179 September, PSR discharge rates vary between 200 and 500 m<sup>3</sup> s<sup>-1</sup>, reaching a  
180 maximum of 2,600 m<sup>3</sup> s<sup>-1</sup> during the rainy period (Silva et al., 2001). The wet  
181 season of 2014 was atypical, due to low precipitation rates caused by sea level  
182 pressure anomalies in Southeastern Brazil, influenced by the La Niña event,  
183 causing extreme rain events.

## 184 **2.2. Sampling**

185 Surface sediment samples (0 - 2 cm) were obtained employing different  
186 techniques, totaling 33 samples distributed into six (hand core sampling), 14  
187 (multicore sampler), and 13 (boxcore sampler) samples from the coastal  
188 Sinnamary River (5°21' - 5°30'N and 52°56' - 53°3'W), the Amazon River (2°S -  
189 4°N and 46° - 51°W), and the PSR (21°28' - 21°40'S and 40°48' - 41°6'W) area,  
190 respectively (Figure 1; Supplementary Table 1). Samples from the Sinnamary  
191 and PSR coastal zones were obtained near mangroves located in the intertidal  
192 estuarine zones, while Amazon samples were collected in the subtidal area  
193 under the influence of the Amazon plume. The sample sets were obtained  
194 during the wet season in January 2019, April 2018, and February 2014 at the  
195 Sinnamary, Amazon, and PSR coastal zones, respectively. The sediments were  
196 immediately frozen (-20 °C) after sampling until further analyses.

197

198 **Figure 1.** South America sediment sampling sites: (A) the Sinnamary estuary,  
199 in the French Guiana (B), the Paraíba do Sul River estuary, in southeastern  
200 Brazil (C) and the Amazon plume, in northern Brazil (D).

201

### 202 **2.3. Elemental and isotopic organic matter compositions**

203 Sediment samples were freeze-dried in the laboratory and  
204 homogenized. For the TOC and  $\delta^{13}\text{C}$  determinations, samples (10 mg) were  
205 acidified in silver capsules for carbonate removal using 2M HCl. For the N and  
206  $\delta^{15}\text{N}$  determinations, samples (10 mg) were weighed into tin capsules.  
207 Elemental and isotopic values were obtained using a Flash 2000 elemental  
208 analyzer coupled to a Delta V mass spectrometer, with an uncertainty of  
209 measurement of 0.05 % for OC, 0.03 % for N, and  $\pm 0.2$  ‰ for  $\delta^{15}\text{N}$  and  $\delta^{13}\text{C}$ .

### 210 **2.4. Black carbon determination**

211 Black carbon contents were determined according to Glaser et al.  
212 (1998) and Brodowski et al. (2005) with slight adaptations. The samples were  
213 pre-digested with 10 mL trifluoroacetic acid for 4 h in a high-pressure system at  
214  $100 \pm 5$  °C, followed by filtering through GF/F filters (Whatman, pore size 0.7  
215  $\mu\text{m}$ ). The filters were then placed in an oven for 2 h at 40 °C. After drying, 2 mL  
216 of nitric acid were added, and the samples were digested at  $165 \pm 5$  °C for 8 h  
217 to obtain BPCAs from OM oxidation. The samples were again filtered through  
218 cellulose acetate filters (pore size 0.2  $\mu\text{m}$ ), and 8 mL of ultrapure water were  
219 added to dilute the applied nitric acid. A total of 50  $\mu\text{L}$  of a surrogate (phthalic  
220 acid, 1 mg  $\text{mL}^{-1}$ ) were added to 2.5 mL sample aliquots to correct for losses  
221 during the cleaning procedure, where the recovery was  $60 \pm 17$  %, indicating  
222 sample losses during the process. Sample purification was conducted  
223 employing columns containing cation exchange resins after conditioning  
224 (Dowex 50 WX 8, 200-400 mesh, Fluka, Steinheim, Germany). The obtained  
225 sample volumes were separated into four vials and freeze-dried, resuspended  
226 with methanol and, finally, dried with  $\text{N}_2$ . The last sample cleaning step

227 consisted in adding 4 mL of pyridine, a centrifugation step, and a new drying  
228 step with N<sub>2</sub>. The samples were then analyzed by gas chromatography (GC-MS)  
229 and ultra-performance liquid chromatography (UPLC), according to Stubbins et al.  
230 (2015). The samples were derivatized for the GC-MS analysis using 250 µL of  
231 pyridine and 250 µL of *N,O*-bis (trimethylsilyl) trifluoroacetamide with 1 %  
232 trimethylchlorosilane (BSTFA-TMCS, 99:1) followed by heating for 2 h at 80 °C  
233 and then injected into the GC-MS. Biphenyl-2,2'-dicarboxylic acid was added as  
234 the internal standard before sample derivatization as an internal calibration of  
235 the GC-MS. Concerning the UPLC analysis, samples were dried with N<sub>2</sub> and  
236 resuspended in a phosphate buffer 100 µL (Na<sub>2</sub>HPO<sub>4</sub> and NaH<sub>2</sub>PO<sub>4</sub> each 5 mM  
237 in ultrapure water, pH 7.2).

238         The correction factor of 1.5 suggested by Schneider et al. (2011) was  
239 used for the samples analyzed via GC-MS to compare the data obtained by the  
240 different approaches since Schneider et al. (2011) reported analytical variability  
241 when comparing gas and liquid chromatography analyses. Other conversion  
242 factors reported for the BPCA method (i.e., Glaser et al., 1998) were not  
243 applied, as also suggested by Schneider et al. (2011). The standard reference  
244 sediment NIST 1941b was used to accurately and precisely determine BPCA  
245 contents. The mean BC content, normalized by the TOC content, detected by  
246 the GC-MS was  $2.08 \pm 0.17 \text{ mg g}^{-1} \text{ TOC}$  ( $n = 5$ ), and the UPLC value was  $2.97$   
247  $\pm 0.26 \text{ mg g}^{-1} \text{ TOC}$  ( $n = 3$ ). The other two digestion products, B3CA and B4CA,  
248 were not assessed, as Kappenberg et al. (2016) demonstrated that these  
249 groups may be produced after the oxidation of non-pyrogenic OM, even when  
250 employing low sample weights (< 5 mg TOC). However, to allow for further  
251 comparisons, we also considered B3CA and B4CA with the conversion factor

252 2.27 from Glaser et al. (1998). Accordingly, the BC/TOC ratios and the BC  
253 contribution for the dry weight sediment found for NIST 1941b were  $1.97 \pm 0.48$   
254 and  $0.05 \pm 0.30$  %, respectively, comparable to previously reported values by  
255 Hammes et al. (2007), with BC accounting for  $0.06 \pm 0.01$  % of the dry sediment  
256 weight and BC/TOC ratios between 2.0 and 8.6.

## 257 **2.5. Organic matter sources**

258 Bayesian mixing models provide a synthesis of source and mixture data  
259 within a model structure that incorporates data variability (e.g., isotopic  
260 fractionation factor) (Parnell et al., 2010; Stock and Semmens, 2016), while  
261 linear mixing models consider that diagenetic changes do not significantly alter  
262  $\delta^{13}\text{C}$  and  $\delta^{15}\text{N}$  OM values. Thus, the Bayesian MixSIAR mixing model was used  
263 to estimate the source contributions of each sample (Stock and Semmens,  
264 2016; Stock et al., 2018). The MixSIAR applied Bayesian isotopic mixing and  
265 fitting models employing Markov chain Monte Carlo (MCMC) simulations of  
266 plausible values consistent with the dataset ( $n = 1,000,000$ , 100,000, and  
267 1,000,000 for the Sinnamary, Amazon, and PSR coastal zones, respectively),  
268 with Gelman diagnostic variables lower than 1.05. Isotopic fractionation factors  
269 used for the models were calculated for each area and possible sources  
270 (Supplementary Table 2). The prior was set as “uninformative”, where prior:  $\alpha =$   
271  $c(1,1,1)$ .

272 Two-endmember (Equation 1) (Schultz and Calder, 1976) and three-  
273 endmember linear models (Equation 2) (Fry, 2013) were used to evaluate the  
274 contributions of common terrestrial sources (terrestrial  $\text{C}_3$  plants) for each  
275 sample to evaluate BC content associations:

276

277 Eq. 1:  $C_3$  plants =  $\left( \frac{\delta^{13}C_{\text{Marine}} - \delta^{13}C_{\text{Sample}}}{\delta^{13}C_{\text{Marine}} - \delta^{13}C_{\text{Terrestrial}}} \right) \cdot 100$

278

279 Where  $\delta^{13}C_{\text{Sample}}$  is equivalent to the value found for a given sample, and  
 280  $\delta^{13}C_{\text{Terrestrial}}$  and  $\delta^{13}C_{\text{Marine}}$  are the isotopic composition values for terrestrial and  
 281 marine sources, respectively. The assumed  $\delta^{13}C$  value for the terrestrial  $C_3$  plant  
 282 endmember was -31.8 ‰ (Martinelli et al., 2021) versus -19.9 ‰ for the marine  
 283 end-member (Bianchi et al., 2018) for the Amazon samples. As potential OM  
 284 sources for the Sinnamary and PSR coastal zones are different, the model  
 285 presenting the respective  $\delta^{13}C$  and  $\delta^{15}N$  values for each area was employed  
 286 through the following equation (2):

287

288 Eq. 2:  $C_3$  plants =  $\frac{(\delta^{15}N_C - \delta^{15}N_B) \cdot (\delta^{13}C_{\text{Sample}} - \delta^{13}C_B) - (\delta^{13}C_C - \delta^{13}C_B) \cdot (\delta^{15}N_{\text{Sample}} - \delta^{15}N_B)}{(\delta^{15}N_C - \delta^{15}N_B) \cdot (\delta^{13}C_A - \delta^{13}C_B) - (\delta^{13}C_C - \delta^{13}C_B) \cdot (\delta^{15}N_A - \delta^{15}N_B)}$

289

290 Where  $\delta^{13}C_{\text{Sample}}$  and  $\delta^{15}N_{\text{Sample}}$  comprise the isotopic composition values  
 291 of the sediment samples. For the Sinnamary coastal zone, A, B, and C represent  
 292 the OM sources originating from terrestrial  $C_3$  plants (mangrove),  
 293 microphytobenthos (MPB), and marine phytoplankton, respectively. The  $\delta^{13}C$  and  
 294  $\delta^{15}N$  values for the assessed mangrove (*Avicennia germinans* litter) were assumed  
 295 to be -30.1 and 2.6 ‰, respectively, versus -20.9 and 4.6 ‰ for MPB (Ray et al.,  
 296 2018). The marine source values during the wet season were -23.9 and 3.4 ‰ for  
 297  $\delta^{13}C$  and  $\delta^{15}N$ , respectively (Matos et al., 2020). Concerning the PSR coastal zone,  
 298 the isotopic compositions of A, B, and C represent terrestrial  $C_3$  plant, marine  
 299 phytoplankton, and terrestrial  $C_4$  plant sources, respectively. The  $\delta^{13}C$  and  $\delta^{15}N$

300 values for the terrestrial C<sub>3</sub> plant source were -31.3 and 2.7 ‰, respectively  
301 (Martinelli et al., 2021). Concerning marine phytoplankton, δ<sup>13</sup>C and δ<sup>15</sup>N values  
302 were -19.0 and 7.5 ‰, respectively (Gatts et al., 2020). The isotopic C and N  
303 values for terrestrial C<sub>4</sub> plants were -14.6 ‰ (Ribas, 2012) and 7.1 ‰ (*internal*  
304 *unpublished data*), respectively.

305 The endmembers used for Equations 1 and 2 were the same as those  
306 employed for the Bayesian Mixing model, chosen based on literature values for  
307 each area, as different environmental settings can affect source isotopic  
308 compositions, such as latitude and altitude. The use of CO<sub>2</sub> by phytoplankton likely  
309 differs between the Sinnamary and Amazon coastal areas, due to distance from  
310 the coast, which could affect the isotopic compositions of the OM sources.  
311 Therefore, marine contributions for the Sinnamary coastal sediments were also  
312 considered, due to mangrove proximity.

## 313 **2.6. Burial Flux**

314 The BC burial fluxes (F<sub>burial</sub>) in coastal sediments were estimated through  
315 Equation (3) (Sánchez-García et al., 2013):

316

317 Eq. 3:  $F_{\text{burial}} = BC \cdot DBD \cdot SAR \cdot (1 - \Phi)$

318

319 Where BC is the sum of B5CA and B6CA (μg g<sup>-1</sup>), DBD is the dry bulk  
320 density (g cm<sup>-3</sup>), and SAR is the sedimentation accumulation rate (cm yr<sup>-1</sup>). The  
321 DBD values were calculated for each sample (Supplementary Table 3). SAR  
322 values were 0.74 (Allison and Lee, 2004) and 0.6 (Wanderley et al., 2013) for the  
323 Sinnamary and PSR coastal zones, respectively. The SAR values differed for the  
324 Amazon set sample (Supplementary Table 3), in agreement with Sobrinho et al.

325 (2021), who grouped four different Amazon continental shelf regions presenting  
326 different deposition rates and sediment structures. Thus, SAR values differed  
327 among samples according to proximity to regions I, II and III (Supplementary Table  
328 1). The central porosity value (0.75) commonly applied for global calculations was  
329 applied (Jönsson et al., 2003) to the Amazon and PSR coastal zones, while 0.5  
330 was applied to the Sinnamary coastal zone, according to Aschenbroich et al.  
331 (2016).

## 332 **2.7. Statistical analyses**

333 Statistical analyses were performed using the R software (R Core Team,  
334 2018). Descriptive statistics comprising medians and interquartile ranges were  
335 employed. Differences in  $\delta^{13}\text{C}$  (‰) values between the evaluated coastal zones  
336 were verified by the Kruskal Wallis test, while BC ( $\text{mg g}^{-1}$  TOC) and B6CA:B5CA  
337 contents were evaluated by an ANOVA test (*aov*, Base Package, R Core Team,  
338 2018) followed by a multiple comparison test (*Tukey HSD*, base package, R Core  
339 Team, 2018) assuming a 95 % confidence level. Model assumptions (normality,  
340 linearity, and residual homoscedasticity) were tested by a maximum likelihood  
341 function (*boxcox*, MASS package, Venables and Ripley, 2002). If a  
342 transformation was indicated by the function, the correct adjustment was  
343 performed. The Pearson correlation analysis was performed to assess potential  
344 correlations between all analyzed parameters (distance from river mouths,  $\delta^{13}\text{C}$ ,  
345 BC, contribution of terrestrial  $\text{C}_3$  plant OM).

346 Furthermore, non-linear regression models were used to evaluate the  
347 associations and behaviors between  $\delta^{13}\text{C}$ , BC and the B6CA:B5CA ratios and  
348 river mouth distances (*lm*, Base Package, R Core Team, 2018). Additionally, a  
349 linear model was constructed to assess associations between BC and the

350 contribution of terrestrial C<sub>3</sub> plants to infer BC sources (*lm*, Base Package, R Core  
351 Team, 2018). Model assumptions (normality, linearity, and residual  
352 homoscedasticity) were tested using a maximum likelihood function (*boxcox*,  
353 MASS package, Venables and Ripley, 2002); when a transformation was indicated  
354 by the function, the correct adjustment was applied.

### 355 **3. RESULTS**

#### 356 **3.1. Organic matter sources**

357 The  $\delta^{13}\text{C}$  values from the coastal zone PSR OM were more <sup>13</sup>C-enriched  
358 ( $-22.6 \pm 1.3$  ‰, Kruskal-Wallis test  $p < 0.01$ ) compared to the Sinnamary and  
359 Amazon River coastal sediments ( $-25.0 \pm 3.1$  and  $-26.1 \pm 1.0$  ‰, respectively)  
360 (Figure 2A; Supplementary Table 2). The  $\delta^{13}\text{C}$  OM values ranged between -27.7  
361 and -25.1 ‰, -32.4 and -20.7 ‰, and -24.8 and -20.4 ‰ for the Sinnamary,  
362 Amazon, and PSR coastal zones, respectively, with a trend towards <sup>13</sup>C  
363 enrichment with increasing distances from the Amazon and PSR river mouths  
364 (Figure 2B).

365

366 **Figure 2.** Boxplots for  $\delta^{13}\text{C}$  OM values ( $n = 6, 14$  and  $13$ , for Sinnamary,  
367 Amazon and PSR coastal zones, respectively) (A) and distribution according to  
368 river mouth distance (log km) (B). Different letters represent statistical  
369 significance for the difference in the means (Kruskal-Wallis tests,  $p < 0.01$ ) and  
370 the circles represent outliers (A). Red symbol values were not used in model  
371 construction.

372

373 The contribution of potential OM sources to the investigated sediment  
374 samples were determined by coupling  $\delta^{13}\text{C}$  and  $\delta^{15}\text{N}$  values (Figure 3A). Bayesian

375 stable isotope mixing models were used to determine OM sources (Figure 3B).  
376 The estimated relative percentages of OM-contributing sources for Sinnamary  
377 River coastal sediments averaged 36.7, 26.4, and 37.0 % for marine sources,  
378 MPB, and terrestrial C<sub>3</sub> plants, respectively. Marine sources accounted for 48.7  
379 % of the OM for Amazon coastal sediments, while terrestrial C<sub>3</sub> plants  
380 presented a significant contribution of 51.3 %. Contributions for PSR coastal  
381 sediments were 39.5 % marine, 35.6 % terrestrial C<sub>3</sub> plants, and 24.9 %  
382 terrestrial C<sub>4</sub> plants.

383

384 **Figure 3.** Cross-plot of  $\delta^{13}\text{C}$  vs  $\delta^{15}\text{N}$  TOC and TN values. Polygons represent  
385 source material and lines represent the discrimination uncertainty (A). Relative  
386 contribution of the different sources for the investigated coastal zones (B). The  
387  $\delta^{13}\text{C}$  source material values were obtained from Ometto et al. (2006), Hamilton and  
388 Lewis (1992), Bouillon et al. (2011), Ray et al. (2018) and Ribas (2012). The  $\delta^{15}\text{N}$   
389 values were obtained from Ometto et al. (2006), Caraballo et al. (2014), Ray et al.  
390 (2018), and Ribas (2012).

391

### 392 **3.2. Black carbon in coastal zones**

393 Black carbon normalized by TOC content differed between the Amazon  
394 ( $0.32 \pm 0.24 \text{ mg g}^{-1} \text{ TOC}$ ) and PSR ( $0.95 \pm 0.74 \text{ mg g}^{-1} \text{ TOC}$ ) coastal zones  
395 (one-way ANOVA:  $p = 0.035$ ), both of which exhibited similar concentrations to  
396 Sinnamary coastal sediments ( $0.73 \pm 0.67 \text{ mg g}^{-1} \text{ TOC}$ ; Figure 4A). In addition,  
397 BC contents were moderately and positively correlated with TOC in the  
398 Sinnamary and Amazon coastal sediments ( $r = 0.60$  and  $0.66$ , respectively;  
399 Supplementary Figure 1) and moderately and negatively correlated with TOC in

400 PSR coastal sediments ( $r = -0.60$ ; Supplementary Figure 1). Concerning the  
401 PSR coastal zone, BC contents generally increased with river mouth distance,  
402 while a strong drop in BC contents was noted for both the Amazon and  
403 Sinnamary coastal sediments, with BC initially increasing followed by a rapid  
404 drop associated to river mouth distance (Figure 4C). The B6CA:B5CA ratios,  
405 used to assess BC degree of condensation, were highest in the PSR coastal  
406 zone samples (one-way ANOVA:  $F = 4.826$ ,  $p < 0.05$ ) compared to the other  
407 investigated coastal zones (Figure 4B). The B6CA:B5CA ratios for the  
408 Sinnamary, Amazon, and PSR sediments were  $0.28 \pm 0.17$ ,  $0.29 \pm 0.23$ , and  
409  $0.50 \pm 0.15$ , respectively (Figure 4B). The trends of the B6CA:B5CA ratios  
410 were not significant (Figure 4D).

411

412 **Figure 4.** Boxplots for BC values normalized to TOC content (A) and  
413 B6CA:B5CA ratios (B) ( $n = 6, 8$  and  $13$ , for Sinnamary, Amazon and PSR  
414 coastal zones, respectively). Relationship between BC content (C) and  
415 B6CA:B5CA ratios (D) concerning distance from the Sinnamary, Amazon, and  
416 PSR River mouths (log km). Letters represent the statistical significances for the  
417 differences in mean values (Tukey's test,  $p < 0.05$ ), and circles represent  
418 outliers (A). Red symbols indicate values that were not used in model  
419 construction.

420

421 Potential BC sources for the investigated coastal zones were inferred  
422 employing the relationship between  $C_3$  plant contributions (Eq. 1 and 2) and  
423 sedimentary OM and BC contents (Figure 5). Black carbon contents increased with

424 increasing C<sub>3</sub> plant OM contributions for the Sinnamary and Amazon coastal  
425 sediments, while the opposite was observed for the PSR.

426

427 **Figure 5.** Contribution of terrestrial C<sub>3</sub> plants to OM vs BC content in  
428 Sinnamary, Amazon, and PSR coastal zone sediments. Data points with red  
429 symbols were not used in model construction.

430 The estimated BC burial fluxes were  $2.19 \pm 2.23$ ,  $0.13 \pm 0.13$  and  $2.39 \pm$   
431  $1.50 \mu\text{g cm}^2 \text{ yr}^{-1}$  for the Sinnamary, Amazon, and PSR coastal zones,  
432 respectively, with the lowest value observed for Amazon coastal zone.

#### 433 **4. DISCUSSION**

##### 434 **4.1. Organic matter coastal sediment sources reflect land-use changes**

435 The detected <sup>13</sup>C enrichment of the PSR coastal sediments represents  
436 a typical signal of terrestrial C<sub>3</sub>-C<sub>4</sub> plant mixtures, reflecting land-use changes in  
437 the PSR drainage basin (Figure 2A). The enrichment of δ<sup>13</sup>C values can be  
438 observed after decades of land-cover changes, decreasing from -25.1 to -20.2  
439 ‰ in 50 years, as described by Vitorello et al. (1989). Ribas (2012) analyzed  
440 vegetation and soil δ<sup>13</sup>C values in the PSR basin and reported that δ<sup>13</sup>C soil and  
441 vegetation samples differed by around 5 ‰. The same trend was observed in  
442 forest areas, with more <sup>13</sup>C enriched soil values. As reported by Boschker and  
443 Middelburg (2002), the difference between forest vegetation and forest soils can  
444 be explained by the preferential use of <sup>12</sup>C compared to <sup>13</sup>C by microorganisms  
445 during OM soil mineralization (Blagodatskaya et al., 2011; Liu and Han, 2021),  
446 while different values for C<sub>4</sub> vegetation and soil can be explained by the land-  
447 use change. Concerning the PSR fluvial system, Marques (2017) reported <sup>13</sup>C-  
448 enriched values ranging from -25 to -23 ‰ for SPM, with C<sub>4</sub> plant contributions

449 ranging from 27 to 40 % to particulate organic carbon, even after centuries of  
450 land-use change (Ribeiro et al., 2009). When reaching the aquatic system, the  
451 particulate organic carbon (POC) receives autochthonous material, such as  
452 from freshwater phytoplankton, with  $\delta^{13}\text{C}$  values according to dissolved  
453 inorganic carbon in the water column used for photosynthesis (Vuorio et al.,  
454 2006). In the estuarine zone, POC  $\delta^{13}\text{C}$  values observed by Marques (2017)  
455 were more  $^{13}\text{C}$  depleted, ranging from -25.8 to -23.7 ‰, indicating mangrove  
456 contributions (terrestrial  $\text{C}_3$  plants) that, in addition to autochthonous  
457 contributions, can dilute terrestrial  $\text{C}_4$  plant contributions to coastal sediments.  
458 Indeed, according to the MixSIAR model, the terrestrial  $\text{C}_3$  plant contribution to  
459 TOC content was higher than that of terrestrial  $\text{C}_4$  plants (Figure 3B), while  
460 marine production was the primary source for PSR coastal sediments. The  
461 marine source being so evident in the mixture of the MO can be attributed to  
462 low river discharge during the sampling period, to low precipitation rates, which  
463 were below 50 % of normally expected values due to a La Niña macroclimatic  
464 event (Marques et al., 2017) and to anthropogenic PSR watershed  
465 modifications (Carvalho et al., 2002; Souza et al., 2010).

466 Sedimentary OM in the Amazon and Sinnamary coastal zones exhibited  
467 a strong  $\text{C}_3$  plant signal, as expected, since local rainforests are dominated by  
468 these types of plants (Figures 1 and 2A). Therefore, the  $^{13}\text{C}$  enrichment noted  
469 for Amazon coastal sediments highlights the increasing contribution of marine  
470 OM sources with increasing river mouth distances (Figure 2B, Supplementary  
471 Figure 1B). The determined sedimentary isotopic C and N composition indicates  
472 that marine sources contributed considerably to several surface sediment  
473 samples (Figure 3A), in line with previous studies demonstrating that offshore

474 TOC is mainly derived from marine primary production (Aller and Blair, 2006;  
475 Sobrinho et al., 2021). Ward et al. (2015) reported that about 50 % of  
476 continental OM does not reach the Amazon coastal zone due to intense OM  
477 river remineralization and sedimentation. In addition, according to Sobrinho et  
478 al. (2021), terrestrial OM that reaches the Amazon River delta comprises the  
479 main OM sediment source. Organic matter is, however, continuously  
480 remineralized in the Amazon River plume and terrestrial OM is replaced by  
481 marine OM, which explains the strong  $^{13}\text{C}$  enrichment noted with increasing  
482 river mouth distances (Aller and Blair, 2006) (Figures 2B and 3B). This trend  
483 has also been reported by Sun et al. (2017), who detected  $^{13}\text{C}$ -enriched isotopic  
484 values ranging from -21.4 and -23.0 ‰ in Amazon fan sediments. Additionally,  
485 by analyzing lignin phenols, these authors also demonstrated that terrestrial OM  
486 reaching the Amazon plume undergoes extensive diagenetic alterations before  
487 being deposited, as previously suggested by Aller and Blair (2006) and Ward et  
488 al. (2015).

489         Sinnamary coastal sediments exhibited a dominance of  $\text{C}_3$  vegetation  
490 (e.g., from the extensive surrounding mangrove, river-transported debris, and  
491 autochthonous production) (Figure 3). When investigating SPM at the  
492 Sinnamary estuary, Ray et al. (2018) reported the same OM source as that  
493 determined in the present study, also reporting significant contributions of the  
494 MPB biofilm to coastal sediments. In addition, a major contribution of terrestrial  
495  $\text{C}_3$  plants was noted by applying the equation model to determine the  
496 contribution for each sample, except for the sample collected near the pioneer  
497 mangrove area, where around 55 % of sediment OM originated from MPB.  
498 Conversely, the surface sediment sample from the adult mangrove area

499 exhibited the lowest MPB contribution (14 %) and the highest terrestrial C<sub>3</sub> plant  
500 contribution (75 %). According to Marchand et al. (2003), the abundance of  
501 MPB biofilms decreases with increasing mangrove age due to decreased light  
502 availability caused by an increased canopy cover, hindering MPB  
503 photosynthesis. This ecological relationship explains the strong negative  
504 correlation observed herein between both sources ( $r = -0.89$ ; Supplementary  
505 Figure 1A).

#### 506 **4.2. Land use BC drivers in coastal zones**

507 Sedimentary BC contents differed between the investigated coastal  
508 zones, with the Amazon presenting lower values (Figure 4A). Indeed, no  
509 pyrogenic material was detected in six of the evaluated Amazon samples  
510 (Supplementary Table 1). The BPCA method includes the polycondensed  
511 aromatic BC fraction but does not detect labile pyrogenic molecules (Wagner et  
512 al., 2021) or the highly condensed fraction (Hammes et al., 2007). In addition,  
513 river mouth distance and river discharge likely play important roles in offshore  
514 BC transport. Less condensed pyrogenic material can be degraded in the fluvial  
515 portion of the land-ocean continuum, as turnover rates may range from days to  
516 weeks (Bird et al., 2015; Wagner et al., 2021). Therefore, the low BC content  
517 determined herein can be explained by dilution due to high river discharges. In  
518 addition, the high residence time of particles in river systems displaying  
519 extensive lowlands, such as the Amazon basin, can result in higher OM  
520 remineralization along the river system (Bianchi et al., 2018). Consequently, BC  
521 can be degraded and replaced by non-thermally modified OM in floodplains  
522 before reaching the coastal zone (Frueh and Lancaster, 2014; Cotrufo et al.,  
523 2016). This degradation in the river section of the land-ocean gradient may

524 explain the low BC content, while the source change of TOC content (terrestrial  
525 to marine) explains the rapid BC content decline with increasing river mouth  
526 distance (Figures 4A and C). The heterogeneity in the B6CA:B5CA ratios along  
527 the land-ocean gradient indicates the presence of two mechanisms acting on  
528 BC deposition in Amazon plume sediments, namely the removal of hydrophobic  
529 components from the dissolved BC fraction by co-precipitation (Coppola et al.,  
530 2014; Coppola et al., 2022), and the remobilization of aged BC from alluvial  
531 sedimentary deposits (Wagner et al., 2018). The first mechanism has been  
532 reported for the North Pacific Ocean, where dissolved BC contributes to  
533 sediment BC content through the adsorption of highly condensed structures  
534 (Nakane et al., 2017). This would explain why the sample with the highest BC  
535 content was the one obtained at the greatest distance to the river mouth. The  
536 second mechanism may be a consequence of energetic mixing and high  
537 particle load of the Amazon River, where particles are subject to numerous  
538 deposition and resuspension cycles during lateral transport. As a result, BC can  
539 be stored in intermediate reservoirs before being stored in marine sediments  
540 (McKee et al., 2004; Coppola et al., 2018).

541         Although the sedimentary BC contents at the Sinnamary River and PSR  
542 coastal zones were comparable, different trends were observed with increasing  
543 river mouth distances (Figures 4A and 4C). In contrast to BC transport along the  
544 Amazon River land-ocean continuum, BC in small to medium-sized rivers such  
545 as the Sinnamary and PSR reaches the coastal zone faster due to the relatively  
546 short time between aquatic system entry and coastal sediment deposition  
547 (Burdige, 2007). Black carbon content seems to be heterogenous in the  
548 Sinnamary coastal zone, with a high BC contribution compared to TOC in two

549 samples collected near the adult mangrove channel and in the middle estuary,  
550 where estuarine mixing takes place (Figure 4C). Mangroves display a high  
551 allochthonous fluvial OM sediment retention capacity (Chew and Gallagher,  
552 2018). Chew and Gallagher (2018) attributed the high BC to TOC ratio detected  
553 in mangrove sediments to fluvial BC transport, as mangroves rarely burn.  
554 Moreover, it is essential to highlight the importance of soot-derived BC canopy  
555 trapping (Agawin and Duarte, 2002; Chew and Gallagher, 2018). In the  
556 estuarine mixing zone, flocculation, and subsequent deposition facilitates the  
557 accumulation of fine particles, resulting in the deposition of thermally and non-  
558 thermally modified OM (Eisma et al., 1994). The removal of hydrophobic  
559 structures from dissolved BC may also explain the increasing B6CA:B5CA  
560 ratios of the sediment samples with increasing river mouth distance, also  
561 observed in the Amazon coastal sediments. The increasing B6CA:B5CA ratios  
562 with increasing distance from the Sinnamary river mouth can also be explained  
563 by atmospheric soot deposition since soot contains the most aromatic form of  
564 BC (Wolf et al., 2013; Saiz et al., 2015; Jones et al., 2017).

565         The BC content increased with increasing distance from the PSR mouth  
566 (Figure 4C and Supplementary Figure 1C), and the evaluated sediments  
567 exhibited higher BC condensation values (Figure 4B), highlighting the refractory  
568 nature of BC in this coastal region. Saiz et al. (2015) observed a higher  
569 production of stable and refractory material in landscapes consisting mainly of  
570 grasses. The same trend observed by Wolf et al. (2013), with B6CA:B5CA  
571 ratios for forest and grass produced from immediate natural fires being  $0.63 \pm$   
572  $0.12$  and  $0.99 \pm 0.27$ , respectively. Thus, the current BC production in the PSR  
573 basin can explain the higher B6CA:B5CA ratios and the stability trend of

574 thermally-modified OM along the land-ocean gradient. By applying the  
575 relationship between BC and the contribution of terrestrial C<sub>4</sub> plants, Marques et  
576 al. (2017) identified historical Atlantic Rainforest burning as the predominant  
577 source of dissolved BC in the PSR, as also suggested by Dittmar et al. (2012a),  
578 with B6CA:B5CA ratios ranging between 0.27 and 0.38. As mentioned  
579 previously, BC soil solubilization and its subsequent entry into the aquatic  
580 system can take decades (Dittmar et al., 2012b). It is therefore expected that  
581 BC originating from historical burning is mobilized from soils mainly by soil OM  
582 solubilization (Dittmar et al., 2012a). Changes in vegetation cover and current  
583 BC production increase soil erosion (Smith et al., 2011), making the input of  
584 particles into the aquatic system more significant for recently produced BC.  
585 When estimating BC content in SPM and dissolved OM, Wagner et al. (2015)  
586 reported an immediate BC contribution to SPM, with a decrease following the  
587 burning event, but increasing again during spring and late summer rain due to  
588 higher runoff. However, land-use fire management in pasture and sugar-cane  
589 areas takes place annually in the PSR basin (Ferreira et al., 2021), continuously  
590 increasing the BC soil pool. Thus, the difference in BC sources and quality  
591 between the sediment compartments in the present study and the dissolved  
592 fraction in Marques et al. (2017) can be explained by differences in molecular  
593 composition modulation for the dissolved and particulate water fractions  
594 (Wagner et al., 2018).

#### 595 **4.3. BC sources and burial fluxes in coastal zones**

596 The thermally modified OM in the sediment compartment of the  
597 evaluated coastal zones varied with the current vegetation cover of each basin  
598 (Figure 5). However, the estimated contribution of C<sub>3</sub> plants does not distinguish

599 vascular plants from autochthonous production in river waters, leading to a  
600 “mixture” factor in the determination coefficient. Historical Atlantic Rainforest  
601 burning explains the dissolved BC concentrations at the PSR (Marques et al.,  
602 2017), although sedimentary BC contents decreased with increasing terrestrial  
603 C<sub>3</sub> OM source contributions in PSR coastal sediments (Figure 5). A high BC  
604 content (2.37 mg g<sup>-1</sup> TOC) detected in one sample without contribution from  
605 terrestrial C<sub>4</sub> plants with a low B6CA:B5CA ratios may indicate the presence of  
606 old BC originating from historical Atlantic Rainforest burning or even from sugar  
607 cane fields that have been fire-managed for centuries in this area (Marques et  
608 al., 2017). Jones et al. (2017) highlighted the importance of atmospheric soot  
609 deposition for BC content in the PSR, indicating that recently produced soot  
610 (e.g., from biomass or fossil fuel burning) can be introduced into the water  
611 column after atmospheric deposition, being subsequently transported along with  
612 river SPM to be deposited in the coastal zone. Thus, in addition to riverine BC  
613 transport, BC can also originate from atmospheric deposition (Lara et al., 2005).  
614 In contrast, atmospheric transport to the Amazon and Sinnamary River mouths  
615 appears to not be significant concerning sedimentary BC contents. According to  
616 Coppola et al. (2019), BC originating from atmospheric deposition can be  
617 rapidly removed or diluted in the fluvial sector of the Amazon River. In the PSR  
618 coastal zone however, a constant BC supply to the coastal zone is directly  
619 linked to the annual fire management of croplands and pasture areas.

620 Black carbon burial flux estimates for coastal zones are important to  
621 better understand the role of thermally modified OM in the global carbon cycle,  
622 as burial in coastal sediments is an essential BC sink (Sánchez-García et al.,  
623 2013; Bird et al., 2015). The burial flux observed for the Amazon coastal zone

624 was significantly lower compared to the other investigated coastal zones (one-  
625 way ANOVA:  $p < 0.001$ ) and was strongly and negatively correlated with  
626 increasing river mouth distance ( $r = -0.88$ ). Similarly, no differences between the  
627 Sinnamary and PSR coastal zones were observed. Including the B3CA and  
628 B4CA markers increased the burial flux for PSR coastal to values between 2.61  
629 and  $306.19 \mu\text{g cm}^{-2} \text{y}^{-1}$ , which is, for example, lower than the burial flux reported  
630 by Sánchez-García et al. (2013) in the Gulf of Cádiz, Spain. However, since  
631 different BC determination methods along the combustion continuum are  
632 available (e.g., including B3CA and B4CA in BC content estimates and/or  
633 applying conversion factors [Glaser et al., 1998]), BC data derived from different  
634 analytical techniques should be compared cautiously (Masiello, 2004;  
635 Schneider et al., 2011; Kappenberg et al., 2016).

636 Black carbon contents can also be associated to organic and inorganic  
637 pollutants (Nam et al., 2008; Liam and Xing, 2017). For example, Neupane et  
638 al. (2020) reported a positive correlation between BC contents (mainly produced  
639 by biomass burning) and Hg concentrations ( $R^2 = 0.48$ ,  $p < 0.001$ ), suggesting  
640 similar sources and/or transport mechanisms in Selin Co lake surface  
641 sediments, located in the central Tibetan Plateau. At the PSR coastal zone, the  
642 constant BC input to the coastal zone is most likely directly associated to the  
643 annual management of croplands and pasture areas (Ferreira et al., 2021) while  
644 Hg is used in the sugar-cane management against pests (Câmara et al., 1986).  
645 Therefore, Hg can be released to the atmosphere by soil volatilization during  
646 the fire management of croplands and pasture areas and, alongside BC, is  
647 transported to aquatic systems, either by fluvial or atmospheric transport.  
648 Moreover, Nam et al. (2008) reported a correlation between BC and persistent

649 organic pollutants, although they emphasized that this relationship could be  
650 masked by the old BC soil stocks. Consequently, understanding BC transport  
651 and burial fluxes will aid in elucidating carbon sinks and also the fate of  
652 contaminants in coastal sediments, especially considering that BC exhibits  
653 environmental persistence.

## 654 **5. CONCLUSIONS**

655 In the present study,  $\delta^{13}\text{C}$  coupled with  $\delta^{15}\text{N}$  analyses and mixing  
656 models were employed to understand the sources, composition, and spatial  
657 dynamics of the organic matter in coastal sediments in northeastern South  
658 American coastal zones in Brazil and French Guiana. Altered vegetation covers  
659 from forests to grasslands were indicated as an OM modification driver in the  
660 investigated coastal sediments. Additionally, we analyzed the contribution of  
661 terrestrial OM ( $\text{C}_3$  plants) to understand BC sources in the assessed drainage  
662 basins. In PSR coastal sediments, a mixture of  $^{13}\text{C}$ -enriched OM derived from  
663  $\text{C}_3$  and  $\text{C}_4$  plants, demonstrated that human-induced modifications from Atlantic  
664 Rainforest to croplands and pasture areas altered the OM composition  
665 transported to the coastal zone. Concerning the BC source for this drainage  
666 basin, we suggest that BC produced from the incomplete burning of terrestrial  
667  $\text{C}_4$  plant biomass is the main BC source for PSR coastal sediments (Figure 5;  
668 Supplementary Figure 1), even though the  $\delta^{13}\text{C}$  analysis was performed on bulk  
669 TOC and not directly on molecular BC markers (BPCA).

670 Remineralization and sedimentation processes along the land-ocean  
671 continuum of the Amazon River coupled to high river discharges can explain the  
672 lower BC contents detected in the Amazon coastal zone compared to the PSR  
673 and Sinnamary study sites. However, this could change in the future due to the

674 high agricultural expansion noted in the Amazon, which could exacerbate social  
675 and ecological impacts in this biome. Over the past 14 years, deforestation and  
676 forest fire rates in the Amazon have reached record levels, with anthropogenic  
677 activities increasingly removing Amazon Rainforest biomass, resulting in  
678 increased BC contents in soil and BC transported to the coastal zone. Even  
679 though land-use changes display the potential to produce more stable BC, it is  
680 crucial to consider that the Amazon rainforest accounts for  $93 \pm 23$  Pg C stored  
681 aboveground, which can substantially increase BC production and lead to  
682 significant carbon cycle impacts.

683

684 **Acknowledgments:** Research in the French Guiana was co-funded by the  
685 French National Agency under the programs "Investissements d'Avenir"  
686 (LabexMER: ANR-10-LABX-19), by the CNRS MITI program ("Pépinière  
687 Interdisciplinaire de Guyane") and by the French Research Institute for  
688 Sustainable Development (IRD). The International GEOTRACES Programme  
689 and support from the U.S. National Science Foundation (Grant OCE-1840868)  
690 to the Scientific Committee on Oceanic Research (SCOR) are also  
691 acknowledged. The German Science Foundation (DFG) is acknowledged for  
692 funding the *R/V Meteor* cruise M147. C.E. Rezende received financial support  
693 from CNPq (305217/2017-8) and FAPERJ (E-26/010.001272/2016 and E-  
694 26/200.893/2021), and this publication is part of his contribution to the INCT  
695 *TMCOcean* on material transfer at the land-ocean interface. T. S. G. Serafim is  
696 grateful for the Master's fellowship from CAPES as well to Heike Simon for all  
697 the support during the BPCA analysis at the Institute for Chemistry and Biology  
698 of the Marine Environment. This research is a GDR LIGA contribution.

699 **6. REFERENCES**

- 700 Agawin, N.S.R., Duarte, C.M., 2002. Evidence of direct particle trapping by a  
701 tropical seagrass meadow. *Estuaries*.  
702 <https://doi.org/10.1007/bf02692217>
- 703 Aller, R.C., 1998. Mobile deltaic and continental shelf muds as suboxic, fluidized  
704 bed reactors. *Marine Chemistry*. [https://doi.org/10.1016/s0304-4203\(98\)00024-3](https://doi.org/10.1016/s0304-4203(98)00024-3)
- 705
- 706 Aller, R.C., Blair, N.E., 2006. Carbon remineralization in the Amazon–Guianas  
707 tropical mobile mudbelt: A sedimentary incinerator. *Continental Shelf*  
708 *Research*. <https://doi.org/10.1016/j.csr.2006.07.016>
- 709 Aller, R.C., Blair, N.E., Xia, Q., Rude, P.D., 1996. Remineralization rates,  
710 recycling, and storage of carbon in Amazon shelf sediments.  
711 *Continental Shelf Research*. [https://doi.org/10.1016/0278-4343\(95\)00046-1](https://doi.org/10.1016/0278-4343(95)00046-1)
- 712
- 713 Aller, R.C., Heilbrun, C., Panzeca, C., Zhu, Z., Baltzer, F., 2004. Coupling  
714 between sedimentary dynamics, early diagenetic processes, and  
715 biogeochemical cycling in the Amazon–Guianas mobile mud belt:  
716 coastal French Guiana. *Marine Geology*.  
717 <https://doi.org/10.1016/j.margeo.2004.04.027>
- 718 Allison, M.A., Lee, M.T., 2004. Sediment exchange between Amazon mudbanks  
719 and shore-fringing mangroves in French Guiana. *Marine Geology*.  
720 <https://doi.org/10.1016/j.margeo.2004.04.026>
- 721 Aragão, L.E.O.C., Anderson, L.O., Fonseca, M.G., Rosan, T.M., Vedovato, L.B.,  
722 Wagner, F.H., Silva, C.V.J., Silva Junior, C.H.L., Arai, E., Aguiar, A.P.,  
723 Barlow, J., Berenguer, E., Deeter, M.N., Domingues, L.G., Gatti, L.,  
724 Gloor, M., Malhi, Y., Marengo, J.A., Miller, J.B., Phillips, O.L., Saatchi,  
725 S., 2018. 21st Century drought-related fires counteract the decline of  
726 Amazon deforestation carbon emissions. *Nature Communication*.  
727 <https://doi.org/10.1038/s41467-017-02771-y>
- 728 Aschenbroich, A., Michaud, E., Stieglitz, T., Fromard, F., Gardel, A., Tavares,  
729 M., & Thouzeau, G., 2016. Brachyuran crab community structure and  
730 associated sediment reworking activities in pioneer and young  
731 mangroves of French Guiana, South America. *Estuarine Coastal and*  
732 *Shelf Science*, 182, 60–71. <https://doi.org/10.1016/j.ecss.2016.09.003>
- 733 Bernardes, M.C., Martinelli, L.A., Krusche, A.V., Gudeman, J., Moreira, M.,  
734 Victoria, R.L., Ometto, J.P.H., Ballester, M.V.R., Aufdenkampe, A.K.,  
735 Richey, J.E., Hedges, J.I., 2004. Riverine organic matter composition as  
736 a function of land use change, Southwest Amazon. *Ecological*  
737 *Applications*. <https://doi.org/10.1890/01-6028>
- 738 Bernini, E., Rezende, C.E., 2004. Estrutura da vegetação em florestas de  
739 mangue do estuário do rio Paraíba do Sul, Estado do Rio de Janeiro,  
740 Brasil. *Acta Botanica Brasilica*. <https://doi.org/10.1590/s0102-33062004000300009>
- 741

- 742 Bianchi, T.S., Cui, X., Blair, N.E., Burdige, D.J., Eglinton, T.I., Galy, V., 2018.  
 743 Centers of organic carbon burial and oxidation at the land-ocean  
 744 interface. *Organic Geochemistry*.  
 745 <https://doi.org/10.1016/j.orggeochem.2017.09.008>
- 746 Bird, M.I., Ascough, P.L., 2012. Isotopes in pyrogenic carbon: A review. *Organic*  
 747 *Geochemistry*. <https://doi.org/10.1016/j.orggeochem.2010.09.005>
- 748 Bird, M.I., Wynn, J.G., Saiz, G., Wurster, C.M., McBeath, A., 2015. The  
 749 Pyrogenic Carbon Cycle. *Annual Review of Earth and Planetary*  
 750 *Sciences*. <https://doi.org/10.1146/annurev-earth-060614-105038>
- 751 Blagodatskaya, E., Yuyukina, T., Blagodatsky, S., Kuzyakov, Y., 2011. Turnover  
 752 of soil organic matter and of microbial biomass under C3–C4 vegetation  
 753 change: Consideration of <sup>13</sup>C fractionation and preferential substrate  
 754 utilization. *Soil Biology and Biochemistry*.  
 755 <https://doi.org/10.1016/j.soilbio.2010.09.028>
- 756 Blair, N.E., Leithold, E.L., Ford, S.T., Peeler, K.A., Holmes, J.C., Perkey, D.W.,  
 757 2003. The persistence of memory: the fate of ancient sedimentary  
 758 organic carbon in a modern sedimentary system. *Geochimica et*  
 759 *Cosmochimica Acta*. [https://doi.org/10.1016/s0016-7037\(02\)01043-8](https://doi.org/10.1016/s0016-7037(02)01043-8)
- 760 Boschker, H.T.S., Middelburg, J.J., 2002. Stable isotopes and biomarkers in  
 761 microbial ecology. *FEMS Microbiology Ecology*.  
 762 <https://doi.org/10.1111/j.1574-6941.2002.tb00940.x>
- 763 Bouillon, S., Connolly, R.M., Gillikin, D.P., 2011. Use of Stable Isotopes to  
 764 Understand Food Webs and Ecosystem Functioning in Estuaries.  
 765 *Treatise on Estuarine and Coastal Science*.  
 766 <https://doi.org/10.1016/b978-0-12-374711-2.00711-7>
- 767 Brodowski, S., Rodionov, A., Haumaier, L., Glaser, B., Amelung, W., 2005.  
 768 Revised black carbon assessment using benzene polycarboxylic acids.  
 769 *Organic Geochemistry*.  
 770 <https://doi.org/10.1016/j.orggeochem.2005.03.011>
- 771 Burdige, D.J., 2007. Preservation of Organic Matter in Marine Sediments:  
 772 Controls, Mechanisms, and an Imbalance in Sediment Organic Carbon  
 773 Budgets? *ChemInform*. <https://doi.org/10.1002/chin.200720266>
- 774 Cai, D.-L., Tan, F.C., Edmond, J.M., 1988. Sources and transport of particulate  
 775 organic carbon in the Amazon River and estuary. *Estuarine, Coastal*  
 776 *and Shelf Science*. [https://doi.org/10.1016/0272-7714\(88\)90008-x](https://doi.org/10.1016/0272-7714(88)90008-x)
- 777 Câmara, V. de M., de M. Câmara, V., Campos, R.C., Perez, M.A., Tambelini,  
 778 A.T., Klein, C.H., 1986. Teores de mercúrio no cabelo: um estudo  
 779 comparativo em trabalhadores da lavoura de cana-de-açúcar com  
 780 exposição pregressa aos fungicidas organo-mercuriais no município de  
 781 Campos - RJ. *Cadernos de Saúde Pública*.  
 782 <https://doi.org/10.1590/s0102-311x1986000300008>
- 783 Caraballo, P., Forsberg, B.R., de Almeida, F.F., Leite, R.G., 2014. Diel patterns  
 784 of temperature, conductivity and dissolved oxygen in an Amazon

785 floodplain lake: description of a friagem phenomenon. *Acta Limnologica*  
786 *Brasiliensia*. <https://doi.org/10.1590/s2179-975x2014000300011>

787 Carvalho, C.E.V., Salomão, M.S.M., Molisani, M.M., Rezende, C.E., Lacerda,  
788 L.D., 2002. Contribution of a medium-sized tropical river to the  
789 particulate heavy-metal load for the South Atlantic Ocean. *Science of*  
790 *The Total Environment*. [https://doi.org/10.1016/s0048-9697\(01\)00869-5](https://doi.org/10.1016/s0048-9697(01)00869-5)

791 Chave, J., Riéra, B., Dubois, M.-A., 2001. Estimation of biomass in a  
792 neotropical forest of French Guiana: spatial and temporal variability.  
793 *Journal of Tropical Ecology*.  
794 <https://doi.org/10.1017/s0266467401001055>

795 Chew, S.T., Gallagher, J.B., 2018. Accounting for black carbon lowers  
796 estimates of blue carbon storage services. *Sci. Rep.* 8, 2553.  
797 <https://doi.org/10.1038/s41598-018-20644-2>

798 Cole, J.J., Prairie, Y.T., Caraco, N.F., McDowell, W.H., Tranvik, L.J., Striegl,  
799 R.G., Duarte, C.M., Kortelainen, P., Downing, J.A., Middelburg, J.J.,  
800 Melack, J., 2007. Plumbing the Global Carbon Cycle: Integrating Inland  
801 Waters into the Terrestrial Carbon Budget. *Ecosystems*.  
802 <https://doi.org/10.1007/s10021-006-9013-8>

803 Coppola, A.I., Seidel, M., Ward, N.D., Viviroli, D., Nascimento, G.S., Haghypour,  
804 N., Revels, B.N., Abiven, S., Jones, M.W., Richey, J.E., Eglinton, T.I.,  
805 Dittmar, T., Schmidt, M.W.I., 2019. Marked isotopic variability within and  
806 between the Amazon River and marine dissolved black carbon pools.  
807 *Nature Communications*. <https://doi.org/10.1038/s41467-019-11543-9>

808 Coppola, A.I., Wagner, S., Lennartz, S.T., Seidel, M., Ward, N.D., Dittmar, T.,  
809 Santín, C., Jones, M.W., 2022. The black carbon cycle and its role in  
810 the Earth system. *Nature Reviews Earth & Environment*.  
811 <https://doi.org/10.1038/s43017-022-00316-6>

812 Coppola, A.I., Wiedemeier, D.B., Galy, V., Haghypour, N., Hanke, U.M.,  
813 Nascimento, G.S., Usman, M., Blattmann, T.M., Reisser, M., Freymond,  
814 C.V., Zhao, M., Voss, B., Wacker, L., Schefuß, E., Peucker-Ehrenbrink,  
815 B., Abiven, S., Schmidt, M.W.I., Eglinton, T.I., 2018. Publisher  
816 Correction: Global-scale evidence for the refractory nature of riverine  
817 black carbon. *Nature Geoscience*. [https://doi.org/10.1038/s41561-018-](https://doi.org/10.1038/s41561-018-0252-z)  
818 [0252-z](https://doi.org/10.1038/s41561-018-0252-z)

819 Coppola, A.I., Ziolkowski, L.A., Masiello, C.A., Druffel, E.R.M., 2014. Aged black  
820 carbon in marine sediments and sinking particles. *Geophysical*  
821 *Research Letters*. <https://doi.org/10.1002/2013gl059068>

822 Cotrufo, M.F., Francesca Cotrufo, M., Boot, C.M., Kampf, S., Nelson, P.A.,  
823 Brogan, D.J., Covino, T., Haddix, M.L., MacDonald, L.H., Rathburn, S.,  
824 Ryan-Bukett, S., Schmeer, S., Hall, E., 2016. Redistribution of  
825 pyrogenic carbon from hillslopes to stream corridors following a large  
826 montane wildfire. *Global Biogeochemical Cycles*.  
827 <https://doi.org/10.1002/2016gb005467>

828 Dittmar, T., 2008. The molecular level determination of black carbon in marine  
829 dissolved organic matter. *Organic Geochemistry*.  
830 <https://doi.org/10.1016/j.orggeochem.2008.01.015>

831 Dittmar, T., de Rezende, C.E., Manecki, M., Niggemann, J., Ovalle, A.R.C.,  
832 Stubbins, A., Bernardes, M.C., 2012a. Continuous flux of dissolved  
833 black carbon from a vanished tropical forest biome. *Nature Geoscience*.  
834 <https://doi.org/10.1038/ngeo1541>

835 Dittmar, T., Paeng, J., Gihring, T.M., Suryaputra, I.G.N., Huettel, M., 2012b.  
836 Discharge of dissolved black carbon from a fire-affected intertidal  
837 system. *Limnology and Oceanography*.  
838 <https://doi.org/10.4319/lo.2012.57.4.1171>

839 Edwards, P.J., 1984. The Use of Fire as a Management Tool. *Ecological*  
840 *Studies*. [https://doi.org/10.1007/978-3-642-69805-7\\_16](https://doi.org/10.1007/978-3-642-69805-7_16)

841 Eisma, D., 1986. Flocculation and de-flocculation of suspended matter in  
842 estuaries. *Netherlands Journal of Sea Research*.  
843 [https://doi.org/10.1016/0077-7579\(86\)90041-4](https://doi.org/10.1016/0077-7579(86)90041-4)

844 Eisma, D., Chen, S., Li, A., 1994. Tidal variations in suspended matter floc size  
845 in the Elbe river and Dollard estuaries. *Netherlands Journal of Aquatic*  
846 *Ecology*. <https://doi.org/10.1007/bf02334194>

847 Ferrante, L., Fearnside, P.M., 2019. Brazil's new president and "ruralists"  
848 threaten Amazonia's environment, traditional peoples and the global  
849 climate. *Environmental Conservation*.  
850 <https://doi.org/10.1017/s0376892919000213>

851 Ferreira, R., Nunes, C., Souza, M., Canela, M., 2021. Multivariate Optimization  
852 of Extraction Variables of PAH in Particulate Matter (PM10) in  
853 Indoor/Outdoor Air at Campos dos Goytacazes, Brazil. *Journal of the*  
854 *Brazilian Chemical Society*. [https://doi.org/10.21577/0103-](https://doi.org/10.21577/0103-5053.20200216)  
855 [5053.20200216](https://doi.org/10.21577/0103-5053.20200216)

856 Figueiredo, R. de O., de Oliveira Figueiredo, R., Ovalle, A.R.C., de Rezende,  
857 C.E., Martinelli, L.A., 2011. Carbon and Nitrogen in the Lower Basin of  
858 the Paraíba do Sul River, Southeastern Brazil: Element fluxes and  
859 biogeochemical processes. *Ambiente e Agua - An Interdisciplinary*  
860 *Journal of Applied Science*. <https://doi.org/10.4136/ambi-agua.183>

861 Forbes, M.S., Raison, R.J., Skjemstad, J.O., 2006. Formation, transformation  
862 and transport of black carbon (charcoal) in terrestrial and aquatic  
863 ecosystems. *Sci. Total Environ.* 370, 190–206.  
864 <https://doi.org/10.1016/j.scitotenv.2006.06.007>

865 Fromard, F., Vega, C., Proisy, C., 2004. Half a century of dynamic coastal  
866 change affecting mangrove shorelines of French Guiana. A case study  
867 based on remote sensing data analyses and field surveys. *Marine*  
868 *Geology*. <https://doi.org/10.1016/j.margeo.2004.04.018>

869 Frueh, W.T., Terry Frueh, W., Lancaster, S.T., 2014. Correction of deposit ages  
870 for inherited ages of charcoal: implications for sediment dynamics  
871 inferred from random sampling of deposits on headwater valley floors.

872 Quaternary Science Reviews.  
873 <https://doi.org/10.1016/j.quascirev.2013.10.029>  
874 Fry, B., 2013. Alternative approaches for solving underdetermined isotope  
875 mixing problems. *Marine Ecology Progress Series*.  
876 <https://doi.org/10.3354/meps10168>  
877 Gallo, M.N., Vinzon, S.B., 2015. Estudo numérico do escoamento em planícies  
878 de marés do canal Norte (estuário do rio Amazonas). *Ribagua*.  
879 <https://doi.org/10.1016/j.riba.2015.04.002>  
880 Gatti, L.V., Basso, L.S., Miller, J.B., Gloor, M., Domingues, L.G., Cassol, H.L.G.,  
881 Tejada, G., Aragão, L.E.O., Nobre, C., Peters, W., Marani, L., Arai, E.,  
882 Sanches, A.H., Corrêa, S.M., Anderson, L., Von Randow, C., Correia,  
883 C.S.C., Crispim, S.P., Neves, R.A.L., 2021. Amazonia as a carbon  
884 source linked to deforestation and climate change. *Nature*.  
885 <https://doi.org/10.1038/s41586-021-03629-6>  
886 Gatts, P.V., Franco, M.A.L., Almeida, M.G., Zalmon, I.R., Di Benedetto, A.P.M.,  
887 Costa, P.A.S., de Rezende, C.E., 2020. The trophic ecology of marine  
888 catfishes in south-eastern Brazil. *Journal of the Marine Biological*  
889 *Association of the United Kingdom*.  
890 <https://doi.org/10.1017/s0025315419001164>  
891 Geyer, W.R., Rockwell Geyer, W., Beardsley, R.C., Lentz, S.J., Candela, J.,  
892 Limeburner, R., Johns, W.E., Castro, B.M., Soares, I.D., 1996. Physical  
893 oceanography of the Amazon shelf. *Continental Shelf Research*.  
894 [https://doi.org/10.1016/0278-4343\(95\)00051-8](https://doi.org/10.1016/0278-4343(95)00051-8)  
895 Glaser, B., Haumaier, L., Guggenberger, G., Zech, W., 1998. Black carbon in  
896 soils: the use of benzenecarboxylic acids as specific markers. *Organic*  
897 *Geochemistry*. [https://doi.org/10.1016/s0146-6380\(98\)00194-6](https://doi.org/10.1016/s0146-6380(98)00194-6)  
898 Goldberg, E.D., 1985. *Black Carbon in the Environment: Properties and*  
899 *Distribution*. John Wiley and Sons, 1985.  
900 Hamilton, S.K., Lewis, W.M., 1992. Stable carbon and nitrogen isotopes in  
901 algae and detritus from the Orinoco River floodplain, Venezuela.  
902 *Geochimica et Cosmochimica Acta*. [https://doi.org/10.1016/0016-](https://doi.org/10.1016/0016-7037(92)90264-j)  
903 [7037\(92\)90264-j](https://doi.org/10.1016/0016-7037(92)90264-j)  
904 Hammes, K., Schmidt, M.W.I., Smernik, R.J., Currie, L.A., Ball, W.P., Nguyen,  
905 T.H., Louchouart, P., Houel, S., Gustafsson, Ö., Elmquist, M.,  
906 Cornelissen, G., Skjemstad, J.O., Masiello, C.A., Song, J., Peng, P. 'an,  
907 Mitra, S., Dunn, J.C., Hatcher, P.G., Hockaday, W.C., Smith, D.M.,  
908 Hartkopf-Fröder, C., Böhmer, A., Lüter, B., Huebert, B.J., Amelung, W.,  
909 Brodowski, S., Huang, L., Zhang, W., Gschwend, P.M., Xanat Flores-  
910 Cervantes, D., Largeau, C., Rouzaud, J.-N., Rumpel, C.,  
911 Guggenberger, G., Kaiser, K., Rodionov, A., Gonzalez-Vila, F.J.,  
912 Gonzalez-Perez, J.A., de la Rosa, J.M., Manning, D.A.C., López-Capel,  
913 E., Ding, L., 2007. Comparison of quantification methods to measure  
914 fire-derived (black/elemental) carbon in soils and sediments using

915 reference materials from soil, water, sediment and the atmosphere.  
916 Global Biogeochemical Cycles. <https://doi.org/10.1029/2006gb002914>  
917 Hedges, J.I., Eglinton, G., Hatcher, P.G., Kirchman, D.L., Arnosti, C., Derenne,  
918 S., Evershed, R.P., Kögel-Knabner, I., de Leeuw, J.W., Littke, R.,  
919 Michaelis, W., Rullkötter, J., 2000. The molecularly-uncharacterized  
920 component of nonliving organic matter in natural environments. *Organic*  
921 *Geochemistry*. [https://doi.org/10.1016/s0146-6380\(00\)00096-6](https://doi.org/10.1016/s0146-6380(00)00096-6)  
922 Jones, M.W., Quine, T.A., de Rezende, C.E., Dittmar, T., Johnson, B., Manecki,  
923 M., Marques, J.S.J., de Aragão, L.E.O.C., 2017. Do Regional Aerosols  
924 Contribute to the Riverine Export of Dissolved Black Carbon? *Journal of*  
925 *Geophysical Research: Biogeosciences*.  
926 <https://doi.org/10.1002/2017jg004126>  
927 Jönsson, A., Gustafsson, Ö., Axelman, J., Sundberg, H., 2003. Global  
928 Accounting of PCBs in the Continental Shelf Sediments. *Environmental*  
929 *Science & Technology*. <https://doi.org/10.1021/es0201404>  
930 Jurado, E., Dachs, J., Duarte, C.M., Simó, R., 2008. Atmospheric deposition of  
931 organic and black carbon to the global oceans. *Atmospheric*  
932 *Environment*. <https://doi.org/10.1016/j.atmosenv.2008.07.029>  
933 Kappenberg, A., Bläsing, M., Lehndorff, E., Amelung, W., 2016. Black carbon  
934 assessment using benzene polycarboxylic acids: Limitations for  
935 organic-rich matrices. *Organic Geochemistry*.  
936 <https://doi.org/10.1016/j.orggeochem.2016.01.009>  
937 Kuehl, S.A., DeMaster, D.J., Nittrouer, C.A., 1986. Nature of sediment  
938 accumulation on the Amazon continental shelf. *Continental Shelf*  
939 *Research*. [https://doi.org/10.1016/0278-4343\(86\)90061-0](https://doi.org/10.1016/0278-4343(86)90061-0)  
940 Kuhlbusch, T.A.J., Crutzen, P.J., 1995. Toward a global estimate of black  
941 carbon in residues of vegetation fires representing a sink of  
942 atmospheric CO<sub>2</sub> and a source of O<sub>2</sub>. *Global Biogeochemical Cycles*.  
943 <https://doi.org/10.1029/95gb02742>  
944 Lara, L., Artaxo, P., Martinelli, L., Camargo, P., Victoria, R., Ferraz, E., 2005.  
945 Properties of aerosols from sugar-cane burning emissions in  
946 Southeastern Brazil. *Atmospheric Environment*.  
947 <https://doi.org/10.1016/j.atmosenv.2005.04.026>  
948 Latrubesse, E.M., 2008. Patterns of anabranching channels: The ultimate end-  
949 member adjustment of mega rivers. *Geomorphology*.  
950 <https://doi.org/10.1016/j.geomorph.2008.05.035>  
951 Laurance, W.F., Albernaz, A.K.M., Da Costa, C., 2001. Is deforestation  
952 accelerating in the Brazilian Amazon? *Environmental Conservation*.  
953 <https://doi.org/10.1017/s0376892901000339>  
954 Lian, F., Xing, B., 2017. Black Carbon (Biochar) In Water/Soil Environments:  
955 Molecular Structure, Sorption, Stability, and Potential Risk.  
956 *Environmental Science & Technology*.  
957 <https://doi.org/10.1021/acs.est.7b02528>

- 958 Liu, J., Han, G., 2021. Tracing Riverine Particulate Black Carbon Sources in  
959 Xijiang River Basin: Insight from Stable Isotopic Composition and  
960 Bayesian Mixing Model. *Water Research*.  
961 <https://doi.org/10.1016/j.watres.2021.116932>
- 962 Lohmann, R., Bollinger, K., Cantwell, M., Feichter, J., Fischer-Bruns, I., Zabel,  
963 M., 2009. Fluxes of soot black carbon to South Atlantic sediments.  
964 *Global Biogeochemical Cycles*. <https://doi.org/10.1029/2008gb003253>
- 965 Major, J., Lehmann, J., Rondon, M., Goodale, C., 2010. Fate of soil-applied  
966 black carbon: downward migration, leaching and soil respiration. *Global  
967 Change Biology*. <https://doi.org/10.1111/j.1365-2486.2009.02044.x>
- 968 Malhi, Y., Roberts, J.T., Betts, R.A., Killeen, T.J., Li, W., Nobre, C.A., 2008.  
969 Climate change, deforestation, and the fate of the Amazon. *Science*  
970 319, 169–172. <https://doi.org/10.1126/science.1146961>
- 971 Malhi, Y., Wood, D., Baker, T.R., Wright, J., Phillips, O.L., Cochrane, T., Meir,  
972 P., Chave, J., Almeida, S., Arroyo, L., Higuchi, N., Killeen, T.J.,  
973 Laurance, S.G., Laurance, W.F., Lewis, S.L., Monteagudo, A., Neill,  
974 D.A., Vargas, P.N., Pitman, N.C.A., Quesada, C.A., Salomão, R., Silva,  
975 J.N.M., Lezama, A.T., Terborgh, J., Martínez, R.V., Vinceti, B., 2006.  
976 The regional variation of aboveground live biomass in old-growth  
977 Amazonian forests. *Global Change Biology*.  
978 <https://doi.org/10.1111/j.1365-2486.2006.01120.x>
- 979 Marchand, C., 2017. Soil carbon stocks and burial rates along a mangrove  
980 forest chronosequence (French Guiana). *Forest Ecology and  
981 Management*. <https://doi.org/10.1016/j.foreco.2016.10.030>
- 982 Marchand, C., Lallier-Vergès, E., Baltzer, F., 2003. The composition of  
983 sedimentary organic matter in relation to the dynamic features of a  
984 mangrove-fringed coast in French Guiana. *Estuarine, Coastal and Shelf  
985 Science*. [https://doi.org/10.1016/s0272-7714\(02\)00134-8](https://doi.org/10.1016/s0272-7714(02)00134-8)
- 986 Marques, J.S.J. (2017). Carbono negro dissolvido no contínuo continente-  
987 oceano no rio Paraíba do Sul (Doctoral dissertation, Tese de  
988 doutorado, Universidade Estadual do Norte Fluminense, 2017).
- 989 Marques, J.S.J., Dittmar, T., Niggemann, J., Almeida, M.G., Gomez-Saez, G.V.,  
990 Rezende, C.E., 2017. Dissolved Black Carbon in the Headwaters-to-  
991 Ocean Continuum of Paraíba Do Sul River, Brazil. *Frontiers in Earth  
992 Science*. <https://doi.org/10.3389/feart.2017.00011>
- 993 Martinelli, L.A., Nardoto, G.B., Soltangheisi, A., Reis, C.R.G., Abdalla-Filho,  
994 A.L., Camargo, P.B., Domingues, T.F., Faria, D., Figueira, A.M.,  
995 Gomes, T.F., Lins, S.R.M., Mardegan, S.F., Mariano, E., Miatto, R.C.,  
996 Moraes, R., Moreira, M.Z., Oliveira, R.S., Ometto, J.P.H., Santos,  
997 F.L.S., Sena-Souza, J., Silva, D.M.L., Silva, J.C.S., Vieira, S.A., 2021.  
998 Determining ecosystem functioning in Brazilian biomes through foliar  
999 carbon and nitrogen concentrations and stable isotope ratios.  
1000 *Biogeochemistry*. <https://doi.org/10.1007/s10533-020-00714-2>

1001 Masiello, C.A., 2004. New directions in black carbon organic geochemistry.  
1002 Marine Chemistry. <https://doi.org/10.1016/j.marchem.2004.06.043>

1003 Matos, C.R.L., Berrêdo, J.F., Machado, W., Sanders, C.J., Metzger, E., Cohen,  
1004 M.C.L., 2020. Carbon and nutrient accumulation in tropical mangrove  
1005 creeks, Amazon region. Marine Geology.  
1006 <https://doi.org/10.1016/j.margeo.2020.106317>

1007 McKee, B.A., Aller, R.C., Allison, M.A., Bianchi, T.S., Kineke, G.C., 2004.  
1008 Transport and transformation of dissolved and particulate materials on  
1009 continental margins influenced by major rivers: benthic boundary layer  
1010 and seabed processes. Continental Shelf Research.  
1011 <https://doi.org/10.1016/j.csr.2004.02.009>

1012 Nakane, M., Ajioka, T., Yamashita, Y., 2017. Distribution and Sources of  
1013 Dissolved Black Carbon in Surface Waters of the Chukchi Sea, Bering  
1014 Sea, and the North Pacific Ocean. Frontiers in Earth Science.  
1015 <https://doi.org/10.3389/feart.2017.00034>

1016 Nam, J.J., Gustafsson, O., Kurt-Karakus, P., Breivik, K., Steinnes, E., Jones,  
1017 K.C., 2008. Relationships between organic matter, black carbon and  
1018 persistent organic pollutants in European background soils: Implications  
1019 for sources and environmental fate. Environmental Pollution.  
1020 <https://doi.org/10.1016/j.envpol.2008.05.027>

1021 Neupane, B., Wang, J., Kang, S., Zhang, Y., Chen, P., Rai, M., Guo, J., Yu, S.,  
1022 Thapa, P., 2020. Black carbon and mercury in the surface sediments of  
1023 Selin Co, central Tibetan Plateau: Covariation with total carbon.  
1024 Science of The Total Environment.  
1025 <https://doi.org/10.1016/j.scitotenv.2020.137752>

1026 Nittrouer, C.A., Curtin, T.B., DeMaster, D.J., 1986. Concentration and flux of  
1027 suspended sediment on the Amazon continental shelf. Continental  
1028 Shelf Research. [https://doi.org/10.1016/0278-4343\(86\)90058-0](https://doi.org/10.1016/0278-4343(86)90058-0)

1029 Oliveira, C. J., & Clavier, J., 2000. Space-time variations of suspended material  
1030 in the Sinnamary estuary, French Guiana: influence of Petit Saut  
1031 electric dam. Revista Brasileira de Oceanografia.  
1032 <https://doi.org/10.1590/S1413-77392000000100003>

1033 Ometto, J.P.H.B., Ometto, J.P.H., Ehleringer, J.R., Domingues, T.F., Berry,  
1034 J.A., Ishida, F.Y., Mazzi, E., Higuchi, N., Flanagan, L.B., Nardoto, G.B.,  
1035 Martinelli, L.A., n.d. The stable carbon and nitrogen isotopic  
1036 composition of vegetation in tropical forests of the Amazon Basin,  
1037 Brazil. Nitrogen Cycling in the Americas: Natural and Anthropogenic  
1038 Influences and Controls. [https://doi.org/10.1007/978-1-4020-5517-1\\_12](https://doi.org/10.1007/978-1-4020-5517-1_12)

1039 Ovalle, A.R.C., Silva, C.F., Rezende, C.E., Gatts, C.E.N., Suzuki, M.S.,  
1040 Figueiredo, R.O., 2013. Long-term trends in hydrochemistry in the  
1041 Paraíba do Sul River, south-eastern Brazil. Journal of Hydrology.  
1042 <https://doi.org/10.1016/j.jhydrol.2012.12.036>

1043 Parnell, A.C., Inger, R., Bearhop, S., Jackson, A.L., 2010. Source partitioning  
1044 using stable isotopes: coping with too much variation. *PLoS One* 5,  
1045 e9672. <https://doi.org/10.1371/journal.pone.0009672>

1046 Ray, R., Michaud, E., Aller, R.C., Vantrepotte, V., Gleixner, G., Walcker, R.,  
1047 Devesa, J., Le Goff, M., Morvan, S., Thouzeau, G., 2018. The sources  
1048 and distribution of carbon (DOC, POC, DIC) in a mangrove dominated  
1049 estuary (French Guiana, South America). *Biogeochemistry*.  
1050 <https://doi.org/10.1007/s10533-018-0447-9>

1051 RC Team. (2018). R Foundation for Statistical Computing, Vienna, Austria,  
1052 2018. R: A language and environment for statistical computing.

1053 Regnier, P., Friedlingstein, P., Ciais, P., Mackenzie, F.T., Gruber, N., Janssens,  
1054 I.A., Laruelle, G.G., Lauerwald, R., Luysaert, S., Andersson, A.J.,  
1055 Arndt, S., Arnosti, C., Borges, A.V., Dale, A.W., Gallego-Sala, A.,  
1056 Godd ris, Y., Goossens, N., Hartmann, J., Heinze, C., Ilyina, T., Joos,  
1057 F., LaRowe, D.E., Leifeld, J., Meysman, F.J.R., Munhoven, G.,  
1058 Raymond, P.A., Spahni, R., Suntharalingam, P., Thullner, M., 2013.  
1059 Anthropogenic perturbation of the carbon fluxes from land to ocean.  
1060 *Nature Geoscience*. <https://doi.org/10.1038/ngeo1830>

1061 Reisser, M., Purves, R.S., Schmidt, M.W.I., Abiven, S., 2016. Pyrogenic Carbon  
1062 in Soils: A Literature-Based Inventory and a Global Estimation of Its  
1063 Content in Soil Organic Carbon and Stocks. *Frontiers in Earth Science*.  
1064 <https://doi.org/10.3389/feart.2016.00080>

1065 Rezende, C.L., Scarano, F.R., Assad, E.D., Joly, C.A., Metzger, J.P.,  
1066 Strassburg, B.B.N., Tabarelli, M., Fonseca, G.A., Mittermeier, R.A.,  
1067 2018. From hotspot to hopespot: An opportunity for the Brazilian  
1068 Atlantic Forest. *Perspectives in Ecology and Conservation*.  
1069 <https://doi.org/10.1016/j.pecon.2018.10.002>

1070 Ribas, L. M. (2012). Caracteriza  o de fontes de mat ria org nica do estu rio  
1071 do rio Para ba do Sul, RJ, Brasil (Doctoral dissertation, Tese de  
1072 doutorado, Universidade Estadual do Norte Fluminense, 2012. Tese  
1073 131p).

1074 Ribeiro, M.C., Metzger, J.P., Martensen, A.C., Ponzoni, F.J., Hirota, M.M.,  
1075 2009. The Brazilian Atlantic Forest: How much is left, and how is the  
1076 remaining forest distributed? Implications for conservation. *Biological  
1077 Conservation*. <https://doi.org/10.1016/j.biocon.2009.02.021>

1078 Richard, S., Arnoux, A., Cerdan, P., Reynouard, C., & Horeau, V., 2000.  
1079 Mercury levels of soils, sediments and fish in French Guiana, South  
1080 America. *Water, Air, and Soil Pollution*, 124(3), 221-244.  
1081 <https://doi.org/10.1023/A:1005251016314>

1082 Richey, J.E., Meade, R.H., Salati, E., Devol, A.H., Nordin, C.F., Dos Santos, U.,  
1083 1986. Water Discharge and Suspended Sediment Concentrations in the  
1084 Amazon River: 1982-1984. *Water Resources Research*.  
1085 <https://doi.org/10.1029/wr022i005p00756>

- 1086 Rodionov, A., Amelung, W., Peinemann, N., Haumaier, L., Zhang, X., Kleber,  
1087 M., Glaser, B., Urusevskaya, I., Zech, W., 2010. Black carbon in  
1088 grassland ecosystems of the world. *Global Biogeochemical Cycles*.  
1089 <https://doi.org/10.1029/2009gb003669>
- 1090 Saiz, G., Wynn, J.G., Wurster, C.M., Goodrick, I., Nelson, P.N., Bird, M.I., 2015.  
1091 Pyrogenic carbon from tropical savanna burning: production and stable  
1092 isotope composition. *Biogeosciences*. <https://doi.org/10.5194/bg-12-1849-2015>
- 1094 Sánchez-García, L., de Andrés, J.R., Gélinas, Y., Schmidt, M.W.I., Louchouart,  
1095 P., 2013. Different pools of black carbon in sediments from the Gulf of  
1096 Cádiz (SW Spain): Method comparison and spatial distribution. *Marine*  
1097 *Chemistry*. <https://doi.org/10.1016/j.marchem.2013.02.006>
- 1098 Schneider, M.P.W., Smittenberg, R.H., Dittmar, T., Schmidt, M.W.I., 2011.  
1099 Comparison of gas with liquid chromatography for the determination of  
1100 benzenepolycarboxylic acids as molecular tracers of black carbon.  
1101 *Organic Geochemistry*.  
1102 <https://doi.org/10.1016/j.orggeochem.2011.01.003>
- 1103 Shultz, D.J., Calder, J.A., 1976. Organic carbon variations in estuarine  
1104 sediments. *Geochimica et Cosmochimica Acta*.  
1105 [https://doi.org/10.1016/0016-7037\(76\)90002-8](https://doi.org/10.1016/0016-7037(76)90002-8)
- 1106 Silva, M.A.L., Calasans, C.F., Ovalle, A.R.C., Rezende, C.E., 2001. Dissolved  
1107 Nitrogen and Phosphorus Dynamics in the Lower Portion of the Paraíba  
1108 do Sul River, Campos dos Goytacazes, RJ, Brazil. *Brazilian Archives of*  
1109 *Biology and Technology*. <https://doi.org/10.1590/s1516-89132001000400006>
- 1111 Singh, N., Abiven, S., Torn, M.S., Schmidt, M.W.I., 2012. Fire-derived organic  
1112 carbon in soil turns over on a centennial scale. *Biogeosciences*.  
1113 <https://doi.org/10.5194/bg-9-2847-2012>
- 1114 Smith, H.G., Sheridan, G.J., Lane, P.N.J., Nyman, P., Haydon, S., 2011.  
1115 Wildfire effects on water quality in forest catchments: A review with  
1116 implications for water supply. *Journal of Hydrology*.  
1117 <https://doi.org/10.1016/j.jhydrol.2010.10.043>
- 1118 Sobrinho, R. de L., de L. Sobrinho, R., Bernardes, M.C., de Rezende, C.E.,  
1119 Kim, J.-H., Schouten, S., Sinninghe Damsté, J.S., 2021. A multiproxy  
1120 approach to characterize the sedimentation of organic carbon in the  
1121 Amazon continental shelf. *Marine Chemistry*.  
1122 <https://doi.org/10.1016/j.marchem.2021.103961>
- 1123 Solórzano, A., de Assis Brasil, L.S.C., de Oliveira, R.R., 2021. The Atlantic  
1124 Forest Ecological History: From Pre-colonial Times to the  
1125 Anthropocene. *The Atlantic Forest*. [https://doi.org/10.1007/978-3-030-55322-7\\_2](https://doi.org/10.1007/978-3-030-55322-7_2)
- 1127 Souza, T.A., Godoy, J.M., Godoy, M.L.D., Moreira, I., Carvalho, Z.L., Salomão,  
1128 M.S.M., Rezende, C.E., 2010. Use of multitracers for the study of water

1129 mixing in the Paraíba do Sul River estuary. *Journal of Environmental*  
1130 *Radioactivity*. <https://doi.org/10.1016/j.jenvrad.2009.11.001>

1131 Stahl, C., Freycon, V., Fontaine, S., Dezécache, C., Ponchant, L., Picon-  
1132 Cochard, C., Klumpp, K., Soussana, J.-F., Blanfort, V., 2016. Soil  
1133 carbon stocks after conversion of Amazonian tropical forest to grazed  
1134 pasture: importance of deep soil layers. *Regional Environmental*  
1135 *Change*. <https://doi.org/10.1007/s10113-016-0936-0>

1136 Stock B.C. and Semmens B.X., 2016. *MixSIAR GUI User Manual*. Version 3.1.  
1137 <https://doi:10.5281/zenodo.1209993>

1138 Stock, B.C., Jackson, A.L., Ward, E.J., Parnell, A.C., Phillips, D.L., Semmens,  
1139 B.X., 2018 Analyzing mixing systems using a new generation of  
1140 Bayesian tracer mixing models.  
1141 <https://doi.org/10.7287/peerj.preprints.26884v1>

1142 Stubbins, A., Spencer, R.G.M., Mann, P.J., Max Holmes, R., McClelland, J.W.,  
1143 Niggemann, J., Dittmar, T., 2015. Utilizing colored dissolved organic  
1144 matter to derive dissolved black carbon export by arctic rivers. *Frontiers*  
1145 *in Earth Science*. <https://doi.org/10.3389/feart.2015.00063>

1146 Sun, S., Schefuß, E., Mulitza, S., Chiessi, C.M., Sawakuchi, A.O., Zabel, M.,  
1147 Baker, P.A., Heffer, J., Mollenhauer, G., 2017. Origin and processing of  
1148 terrestrial organic carbon in the Amazon system: lignin phenols in river,  
1149 shelf, and fan sediments. *Biogeosciences*. <https://doi.org/10.5194/bg-14-2495-2017>

1151 Venables, W.N., Ripley, B.D., 2002. *Modern Applied Statistics with S*. *Statistics*  
1152 *and Computing*. <https://doi.org/10.1007/978-0-387-21706-2>

1153 Vitorello, V.A., Cerri, C.C., Andreux, F., Feller, C., Victória, R.L., 1989. Organic  
1154 Matter and Natural Carbon-<sup>13</sup> Distribution in Forested and Cultivated  
1155 Oxisols. *Soil Science Society of America Journal*.  
1156 <https://doi.org/10.2136/sssaj1989.03615995005300030024x>

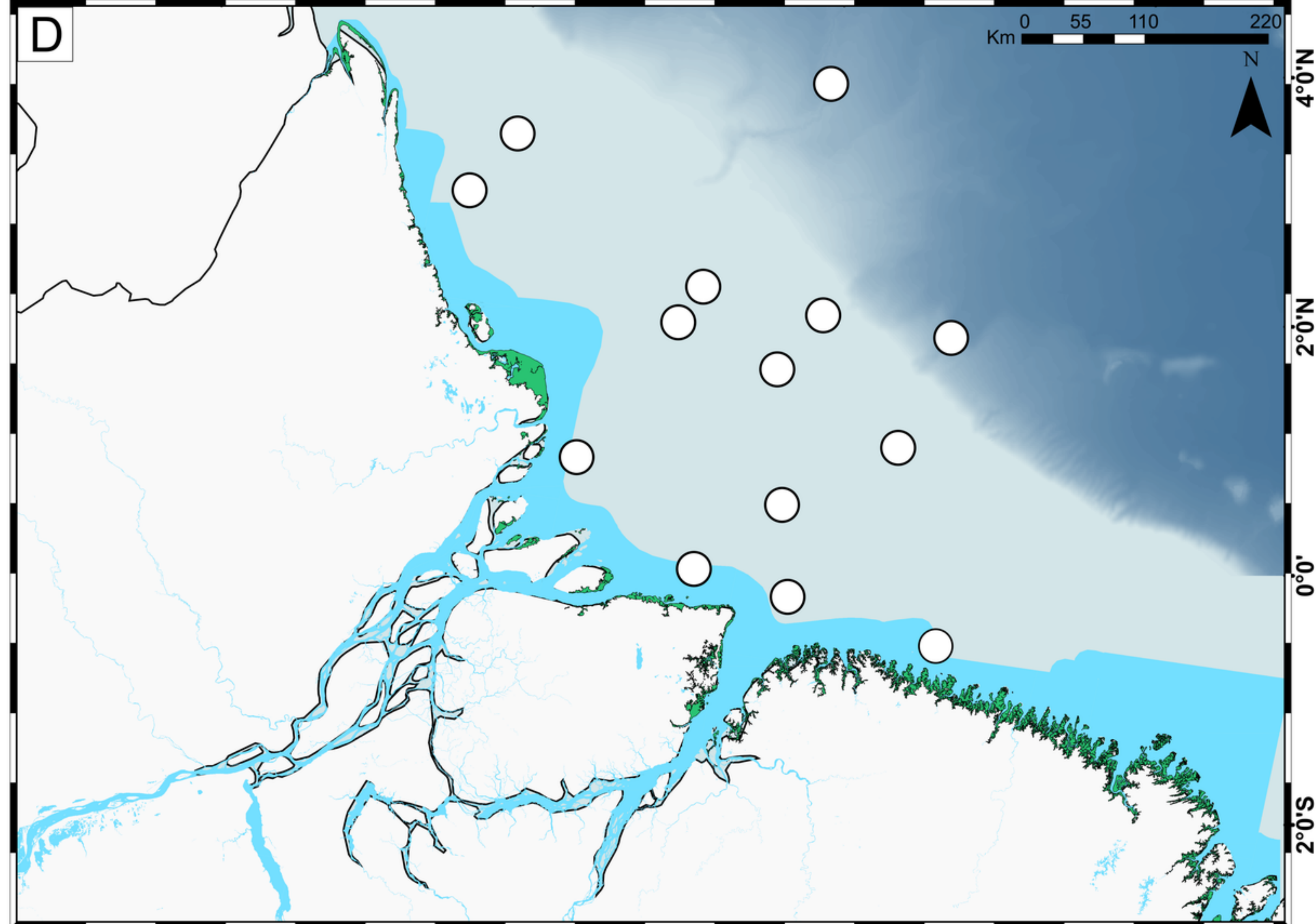
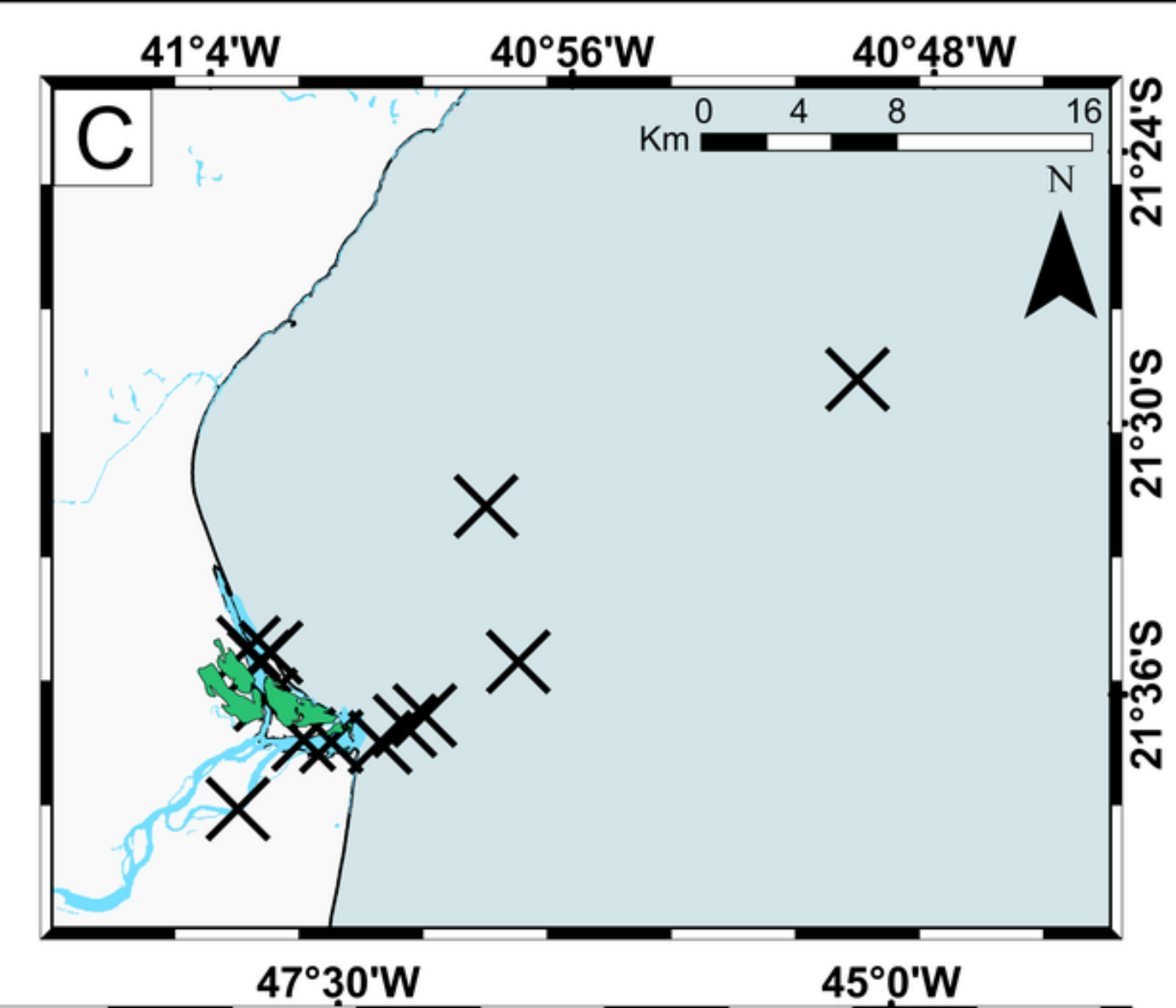
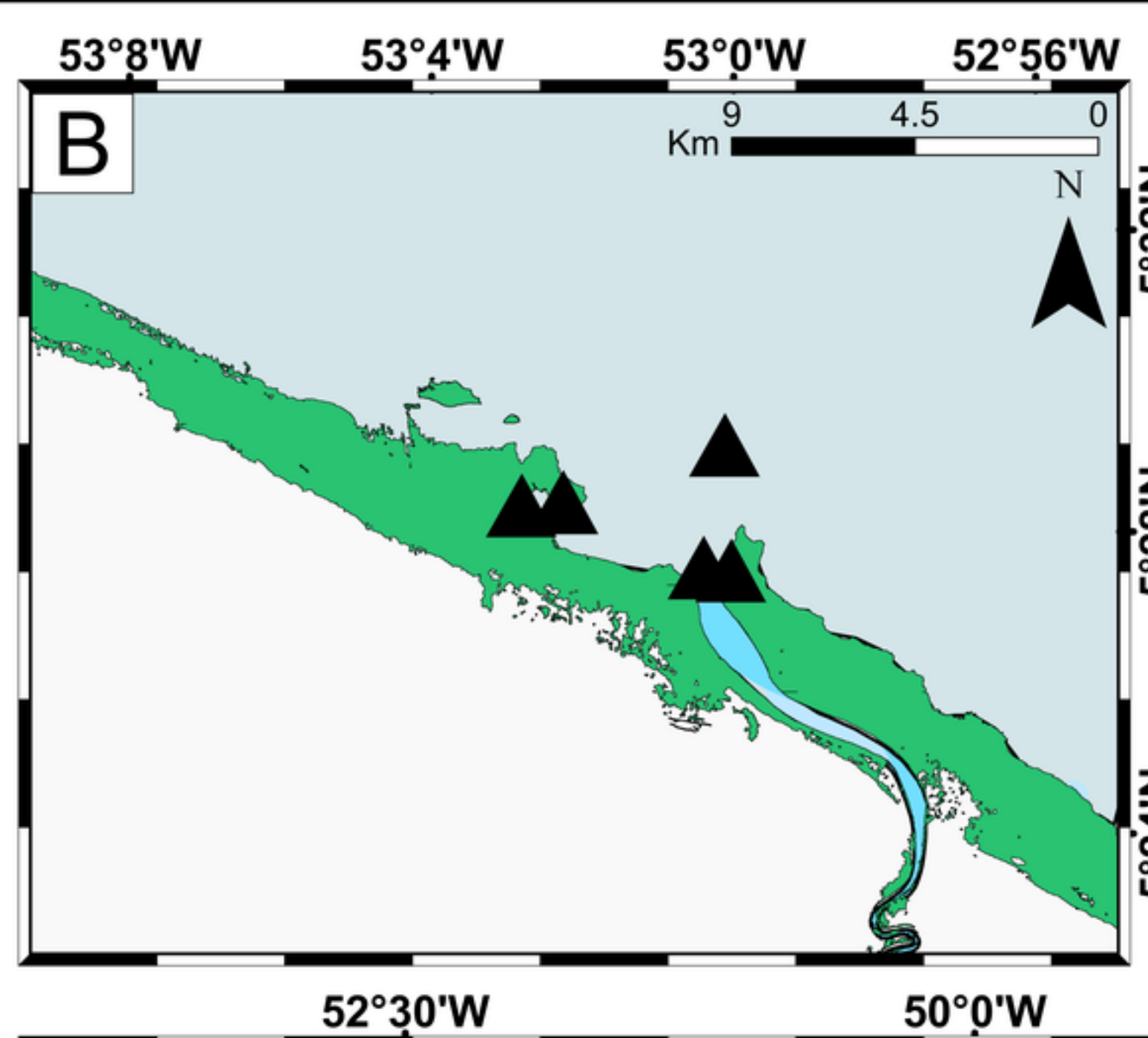
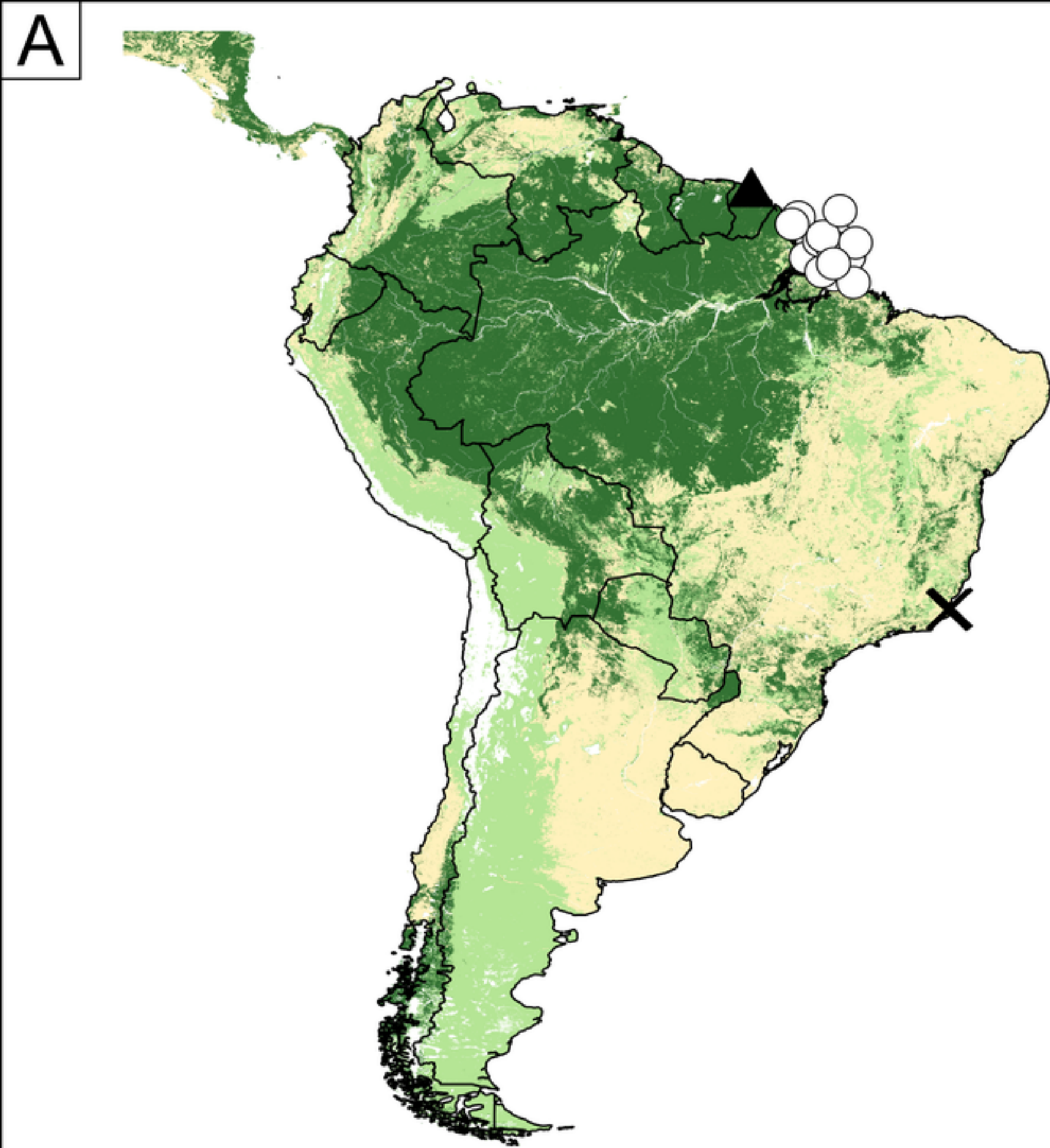
1157 Vuorio, K., Meili, M., Sarvala, J., 2006. Taxon-specific variation in the stable  
1158 isotopic signatures ( $\delta^{13}\text{C}$  and  $\delta^{15}\text{N}$ ) of lake phytoplankton. *Freshwater*  
1159 *Biology*. <https://doi.org/10.1111/j.1365-2427.2006.01529.x>

1160 Wagner, S., Cawley, K.M., Rosario-Ortiz, F.L., Jaffé, R., 2015. In-stream  
1161 sources and links between particulate and dissolved black carbon  
1162 following a wildfire. *Biogeochemistry*. <https://doi.org/10.1007/s10533-015-0088-1>

1164 Wagner, S., Coppola, A.I., Stubbins, A., Dittmar, T., Niggemann, J., Drake,  
1165 T.W., Seidel, M., Spencer, R.G.M., Bao, H., 2021. Questions remain  
1166 about the biolability of dissolved black carbon along the combustion  
1167 continuum. *Nature Communications*. <https://doi.org/10.1038/s41467-021-24477-y>

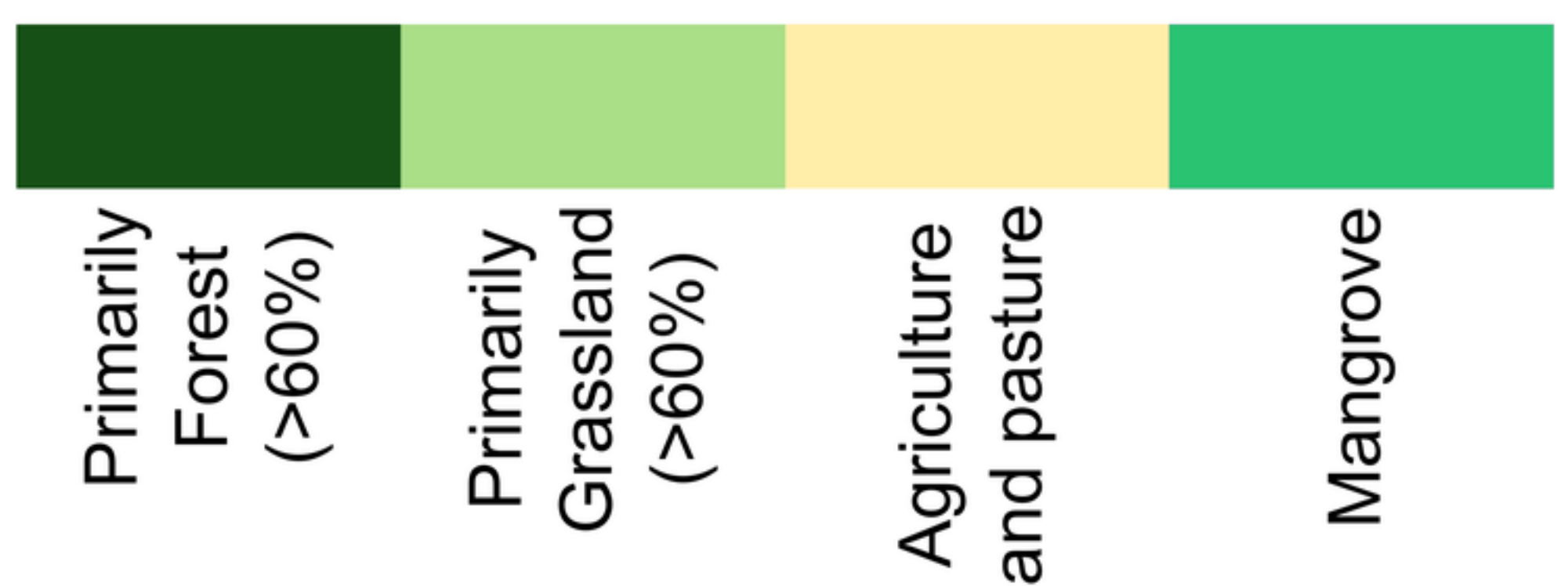
1169 Wagner, S., Jaffé, R., Stubbins, A., 2018. Dissolved black carbon in aquatic  
1170 ecosystems. *Limnology and Oceanography Letters*.  
1171 <https://doi.org/10.1002/lol2.10076>

- 1172 Wanderley, C.V.A., Godoy, J.M., Godoy, M.L.D., Rezende, C.E., Lacerda, L.D.,  
1173 Moreira, I., Carvalho, Z.L., 2013. Evaluating Sedimentation Rates in the  
1174 Estuary and Shelf Region of the Paraíba do Sul River, Southeastern  
1175 Brazil. *Journal of the Brazilian Chemical Society*.  
1176 <https://doi.org/10.5935/0103-5053.20130268>
- 1177 Ward, N.D., Krusche, A.V., Sawakuchi, H.O., Brito, D.C., Cunha, A.C., Moura,  
1178 J.M.S., da Silva, R., Yager, P.L., Keil, R.G., Richey, J.E., 2015. The  
1179 compositional evolution of dissolved and particulate organic matter  
1180 along the lower Amazon River—Óbidos to the ocean. *Marine*  
1181 *Chemistry*. <https://doi.org/10.1016/j.marchem.2015.06.013>
- 1182 Wells, J.T., Coleman, J.M., 1981. Periodic mudflat progradation, northeastern  
1183 coast of South America; a hypothesis. *Journal of Sedimentary*  
1184 *Research*. <https://doi.org/10.2110/jsr.51.1069>
- 1185 Werf, G.R. van der, van der Werf, G.R., Randerson, J.T., Giglio, L., van  
1186 Leeuwen, T.T., Chen, Y., Rogers, B.M., Mu, M., van Marle, M.J.E.,  
1187 Morton, D.C., James Collatz, G., Yokelson, R.J., Kasibhatla, P.S., 2017.  
1188 Global fire emissions estimates during 1997–2016. *Earth System*  
1189 *Science Data*. <https://doi.org/10.5194/essd-9-697-2017>
- 1190 Wilkinson, B.H., McElroy, B.J., 2007. The impact of humans on continental  
1191 erosion and sedimentation. *Geological Society of America Bulletin*.  
1192 <https://doi.org/10.1130/b25899>
- 1193 Wolf, M., Lehndorff, E., Wiesenberg, G.L.B., Stockhausen, M., Schwark, L.,  
1194 Amelung, W., 2013. Towards reconstruction of past fire regimes from  
1195 geochemical analysis of charcoal. *Organic Geochemistry*.  
1196 <https://doi.org/10.1016/j.orggeochem.2012.11.002>

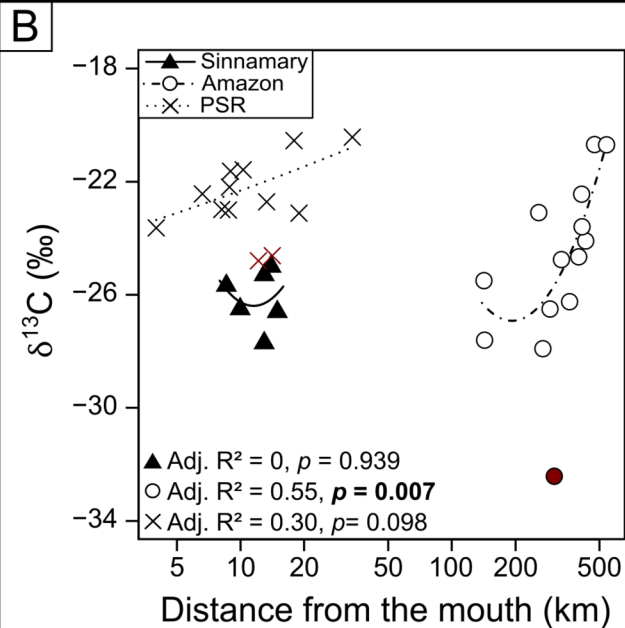
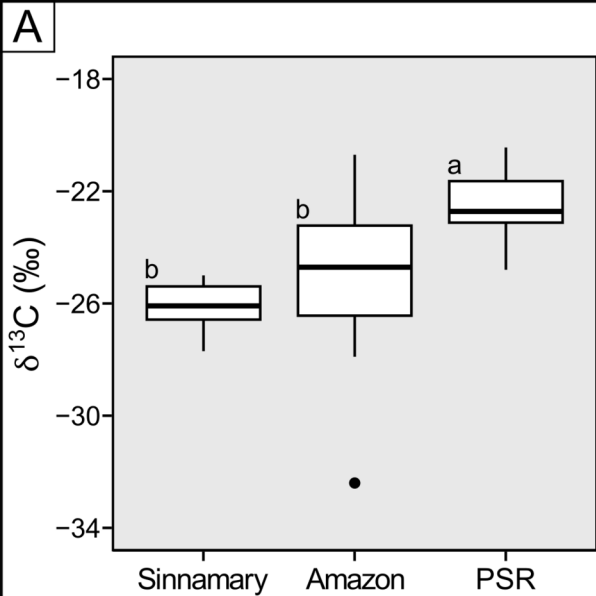


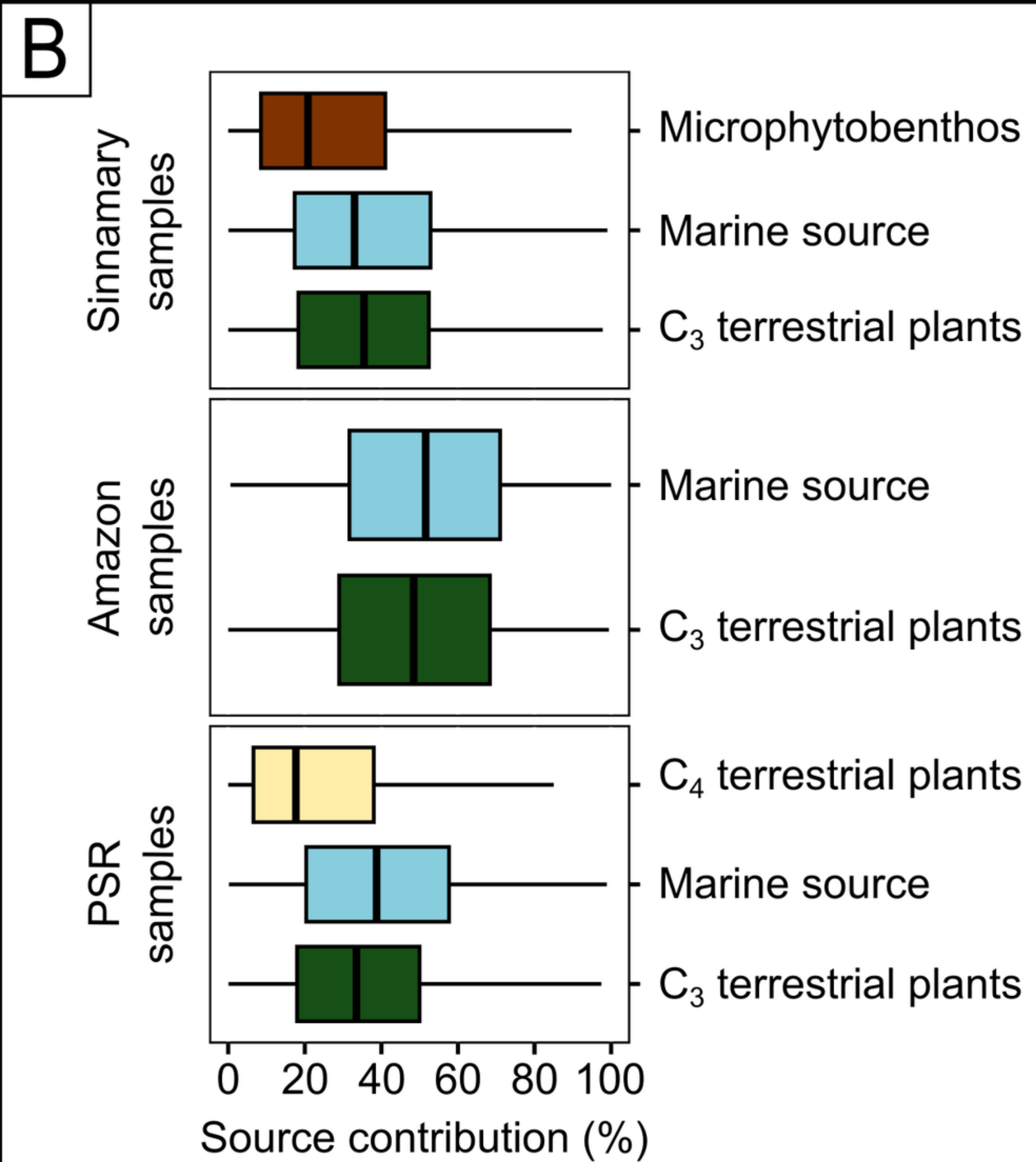
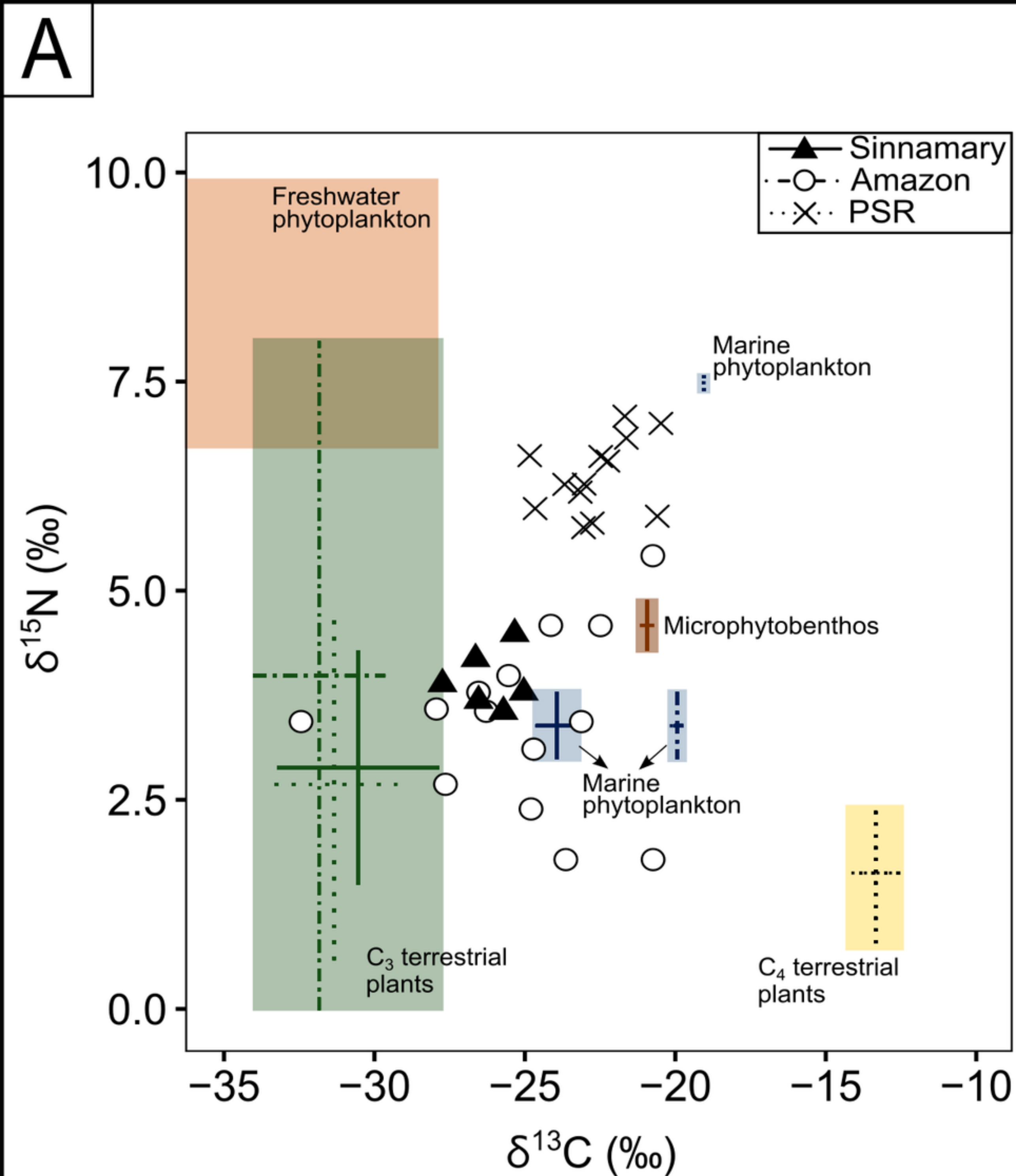
- ▲ Sinnamary coastal zone, French Guiana
- Amazon coastal zone, Brazil
- × Paraíba do Sul coastal zone, Brazil

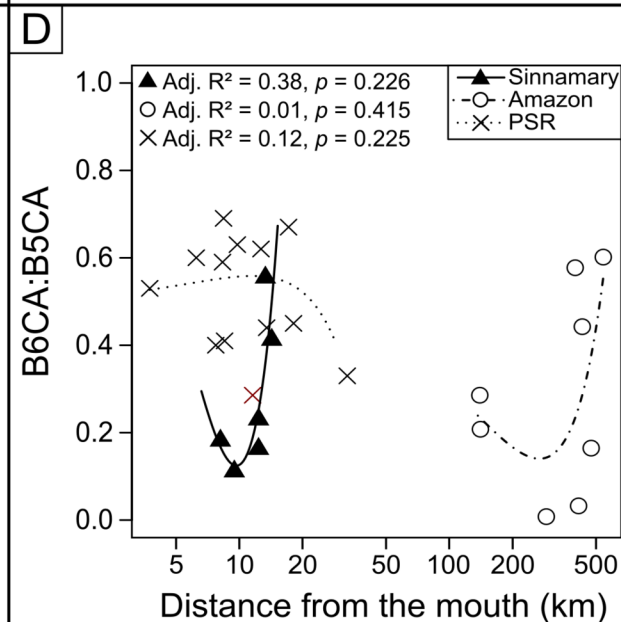
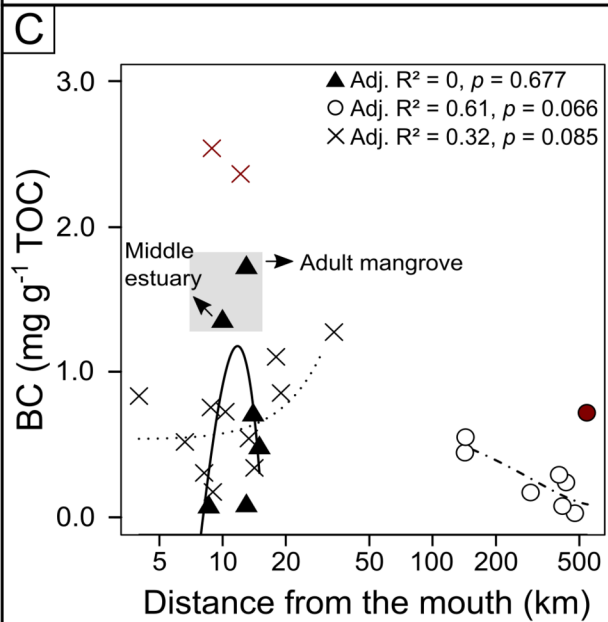
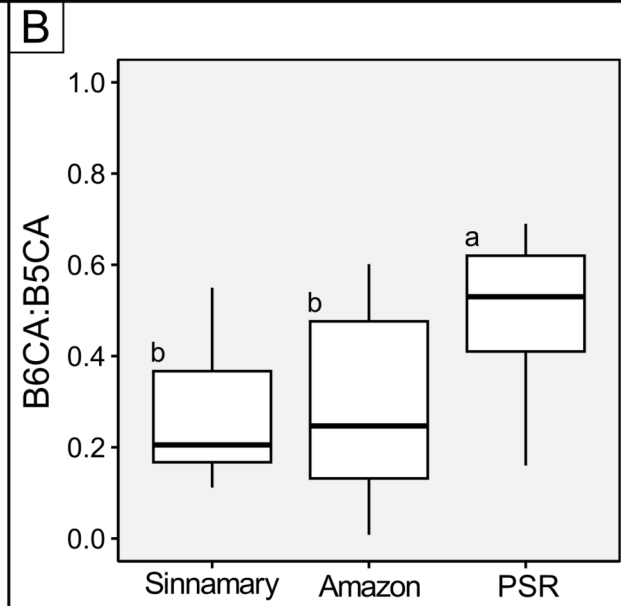
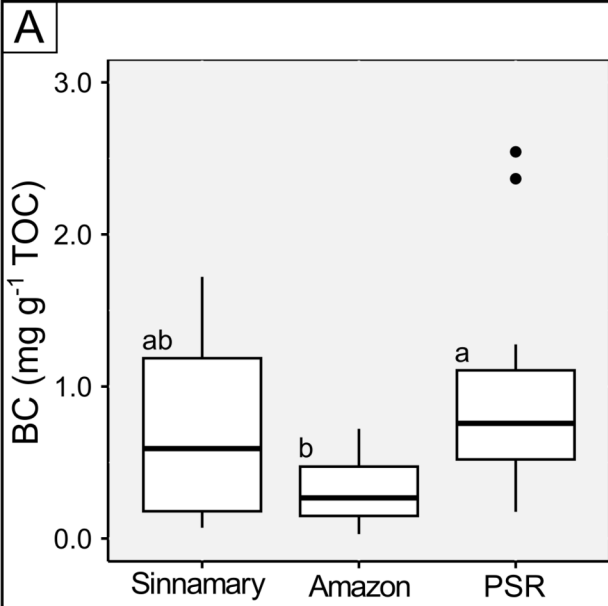
**Land cover**

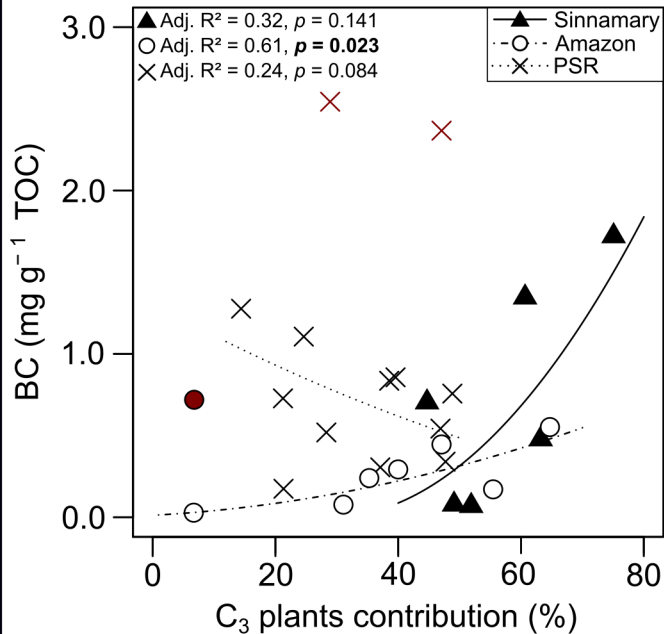


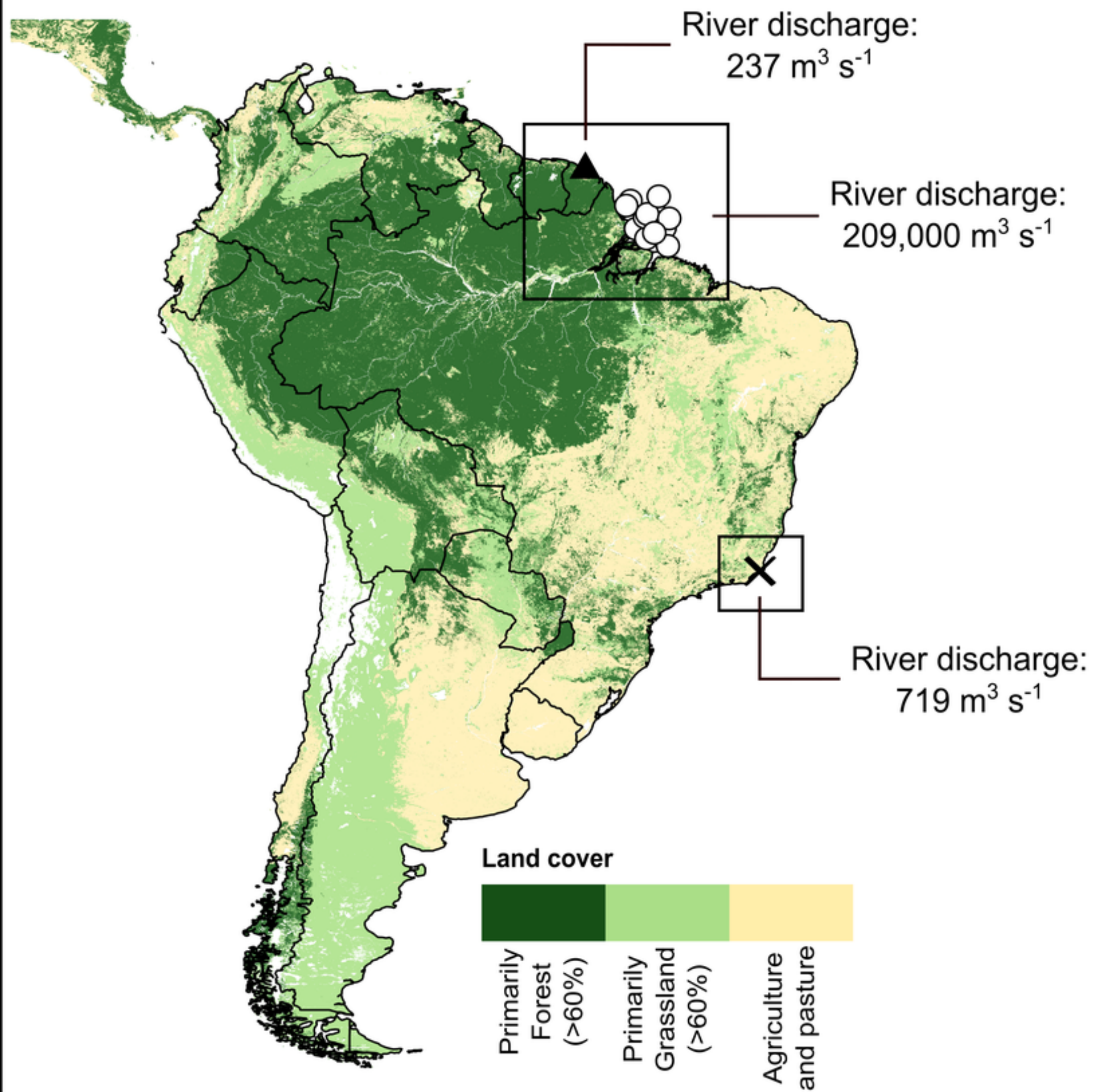
Coordinate System: GCS Sirgas2000; Datum: Sirgas2000  
 Source: ESRI, IGN, IBGE, SRTM, INPE, IFPRI



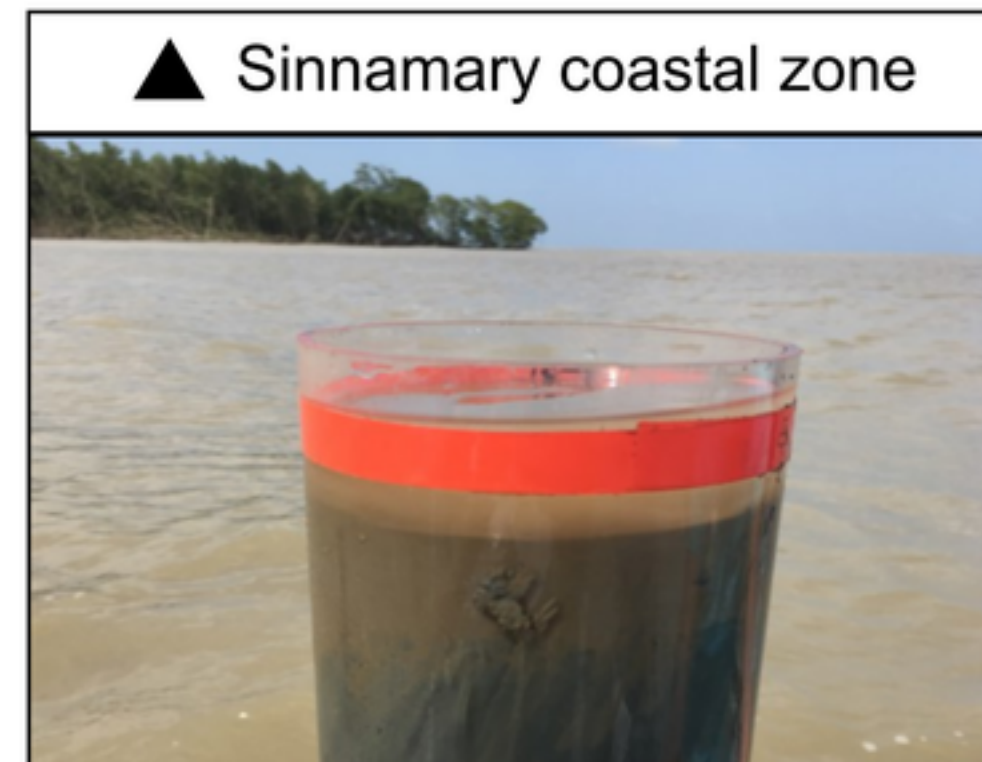








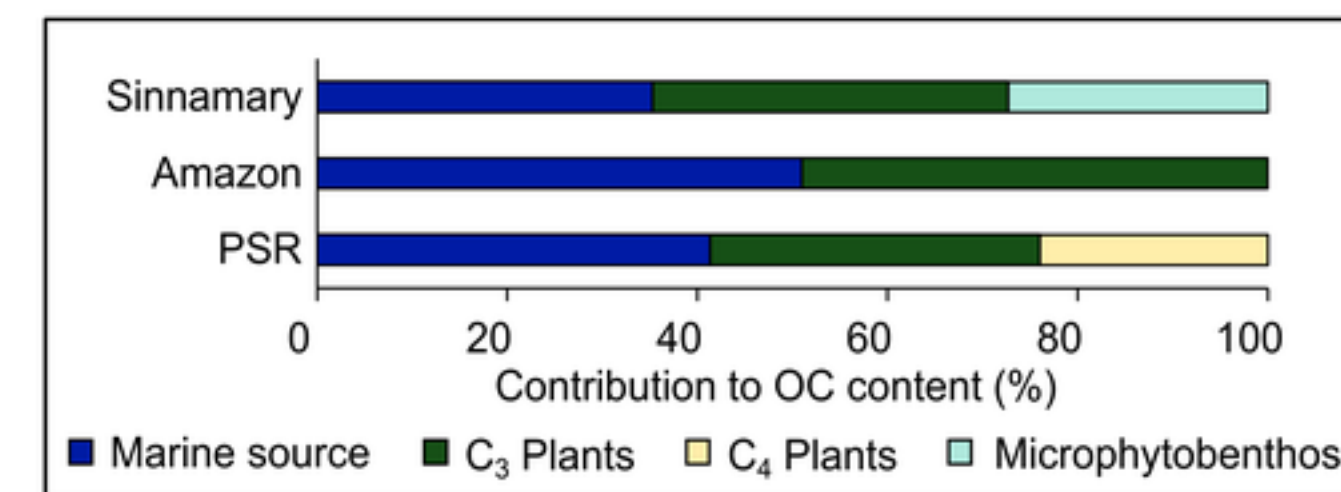
Coastal sediment samples



Bulk organic carbon

- ▲  $\delta^{13}\text{C}$ :  $-25.0 \pm 3.1$  ‰
- $\delta^{13}\text{C}$ :  $-26.1 \pm 1.0$  ‰
- ×  $\delta^{13}\text{C}$ :  $-22.6 \pm 1.3$  ‰ → <sup>13</sup>C-enriched

MixSIAR models



Black carbon

- ▲ BC:  $0.73 \pm 0.67$  mg g<sup>-1</sup> TOC
  - BC:  $0.32 \pm 0.24$  mg g<sup>-1</sup> TOC
  - × BC:  $0.95 \pm 0.74$  mg g<sup>-1</sup> TOC
- $p = 0.043$

- ▲ B6CA:B5CA:  $0.28 \pm 0.17$
- B6CA:B5CA:  $0.29 \pm 0.23$
- × B6CA:B5CA:  $0.50 \pm 0.15$  → Higher degree of condensation